

# New and improved rotational periods of magnetic CP stars from ASAS-3, KELT and MASCARA data

Klaus Bernhard,<sup>1,2\*</sup> Stefan Hümmerich,<sup>1,2</sup> Ernst Paunzen<sup>3</sup>

<sup>1</sup>*Bundesdeutsche Arbeitsgemeinschaft für Veränderliche Sterne e.V. (BAV), Berlin, Germany*

<sup>2</sup>*American Association of Variable Star Observers (AAVSO), Cambridge, USA*

<sup>3</sup>*Department of Theoretical Physics and Astrophysics, Masaryk University, Kotlářská 2, 611 37 Brno, Czech Republic*

Accepted XXX. Received YYY; in original form ZZZ

## ABSTRACT

Magnetic chemically peculiar (mCP) stars allow the investigation of such diverse phenomena as atomic diffusion, magnetic fields and stellar rotation. The aim of the present investigation is to enhance our knowledge of the rotational properties of mCP stars by increasing the sample of objects with accurately determined rotational periods. To this end, archival photometric time-series data from the ASAS-3, KELT and MASCARA surveys were employed to improve existing rotational period information and derive rotational periods for mCP stars hitherto not known to be photometric variables. Our final sample consists of 294 mCP stars, a considerable amount of which (more than 40%) are presented here as photometric variables for the first time. In addition, we identified 24 mCP star candidates that show light variability in agreement with rotational modulation but lack spectroscopic confirmation. The rotational period distribution of our sample agrees well with the literature. Most stars are between 100 Myr and 1 Gyr old, with an apparent lack of very young stars. No objects were found on the zero age main sequence; several stars seem to have evolved to the subgiant stage, albeit well before the first dredge-up. We identified four eclipsing binaries (HD 244391, HD 247441, HD 248784 and HD 252519), which potentially host an mCP star. This is of great interest because mCP stars are very rarely found in close binary systems, particularly eclipsing ones. Using archival spectra, we find strong evidence that the HD 252519 system indeed harbours an mCP star component.

**Key words:** stars: chemically peculiar – stars: variables: general – stars: rotation

## 1 INTRODUCTION

Chemically peculiar (CP) stars form a significant fraction (about 10%) of upper main-sequence stars and are mostly found between spectral types early B to early F. The magnetic Of?p stars extend this range to spectral types of early O (Wade et al. 2011a,b); they are, however, rare objects. The defining characteristic of CP stars is the presence of spectral peculiarities, which indicate unusual elemental abundance patterns. Several groups of CP stars have been defined, such as the metallic-line or Am (CP1) stars, the magnetic Bp/Ap (CP2) stars, the Mercury-Manganese (HgMn/CP3) stars, the He-weak (CP4) stars or the  $\lambda$  Bootis stars (Preston 1974; Maitzen 1984; Paunzen 2004; Ghazaryan et al. 2018).

Relevant to the present investigation is the group of the magnetic CP (mCP) stars that traditionally consists

of the CP2 stars and the He-peculiar (CP4 and He-rich) stars. These stars possess strong (up to several tens of kG; Aurière et al. 2007) and organized magnetic fields and exhibit characteristic abundance anomalies that are generally thought to be the result of the competition between radiative levitation and gravitational settling (atomic diffusion; Michaud 1970; Richer et al. 2000). The class-defining characteristics of the He-peculiar stars are their strong or weak lines of neutral He. In addition, certain other peculiarities, such as photospheric overabundances of Si, P, Ga, Sr or Ti in the He-weak stars, may be present. The CP2 stars show greatly enhanced abundances of certain elements like Si, Fe, Sr, Cr, and the rare-earth elements, whose absorption lines in the blue-violet spectral region are traditionally used for a classification of these objects (Preston 1974). CP2 stars also show significant, though scattered, underabundances of He and quite often peculiarly weak or strong Ca II K lines, which renders spectral classification difficult (Gray & Corbally 2009; Ghazaryan et al. 2018).

\* E-mail: klaus.bernhard@liwest.at

Likely due to the influence of the magnetic field on the diffusion processes, mCP stars show a non-uniform distribution of chemical elements (chemical spots or belts) on their surfaces. Flux is redistributed in the abundance patches (line and continuum blanketing; for details cf. e.g. [Lanz et al. 1996](#); [Shulyak et al. 2010](#)) and mCP stars show strictly periodic light, spectral, and magnetic variations with the rotation period, which are well understood in terms of the oblique-rotator model in which the magnetic axis is oblique to the rotation axis ([Stibbs 1950](#)). According to convention, photometrically variable mCP stars are also referred to, after their bright prototype, as  $\alpha^2$  Canum Venaticorum (ACV) variables.

The observed amplitudes of the light variations in ACV variables are generally of the order of only several hundredth of a magnitude in the optical region, reaching up to more than 0.1 mag ( $V$ ) in rare instances. However, analyzing photometric time-series data is an efficient means of deriving information on the rotational period, in particular as they are much easier acquired than spectroscopic time series. Many studies have successfully exploited the wealth of archival photometric observations provided by numerous past and on-going sky surveys ([Paunzen & Maitzen 1998](#); [Wraight et al. 2012](#); [Bernhard et al. 2015a,b](#); [Hümmerich et al. 2016](#); [Bowman et al. 2018](#); [Hümmerich et al. 2018](#); [David-Uraz et al. 2019](#); [Sikora et al. 2019](#)), which has greatly enhanced our knowledge of the rotational properties of mCP stars (e.g. [Netopil et al. 2017](#)).

The present investigation's aim is to add to our knowledge of the rotational properties of mCP stars by increasing the sample of these objects with accurately determined rotational periods, thereby continuing our efforts in this respect ([Paunzen & Maitzen 1998](#); [Bernhard et al. 2015a,b](#); [Hümmerich et al. 2016, 2018](#)). To this end, archival photometric time-series data were employed to (i) improve existing rotational period information and (ii) derive rotational periods for stars hitherto not known to be photometric variables / ACV variables. Our final sample consists of 318 stars: 294 mCP stars, a considerable amount of which (more than 40%) are presented here as photometric variables for the first time, and 24 mCP star candidates.

We have identified four eclipsing binary systems among our targets, which are potentially of great interest because mCP stars are very rarely found in close binary systems, particularly eclipsing ones ([Renson & Manfroid 2009](#); [Niemczura et al. 2017](#); [Kochukhov et al. 2018](#)). Using archival spectra, we find strong evidence that the system of HD 252519 indeed harbours an mCP star component; all other systems should be investigated with time-resolved spectroscopy for confirmation.

The employed photometric time-series data, the process of target selection and the methods of data analysis and classification are described in Section 2. Results are presented in Section 3, which also discusses the eclipsing binary systems in more detail. We conclude in Section 4.

## 2 OBSERVATIONS, TARGET SELECTION AND DATA ANALYSIS

This section contains a short description of the photometric survey sources employed in the present study. Further detailed information can be gleaned from the references given. In addition, we detail the processes of target selection, data analysis and classification that led to the here presented sample of mCP stars and candidates.

### 2.1 Observations

#### 2.1.1 The All Sky Automated Survey (ASAS)

The All Sky Automated Survey (ASAS)<sup>1</sup> constantly monitored the entire southern sky and part of the northern sky to about  $\delta < +28^\circ$ , with the goal of detecting and analyzing any kind of photometric variability. In the present study, data from the third phase of the project (ASAS-3) have been employed, which lasted from 2000 until 2009 ([Pojmanski 2002](#)). Observations were procured at the 10-inch astrograph dome of the Las Campanas Observatory, Chile with two wide-field telescopes equipped with f/2.8 200 mm Minolta lenses and 2048 x 2048 AP 10 Apogee CCD cameras (field of view of  $8^\circ.8 \times 8^\circ.8$ ). Observations were acquired in Johnson ( $V$ ) and reasonable photometry is available for stars in the magnitude range from 7 to 14. The strict observing cadence of the ASAS survey (typically one observation per day; [Pigulski 2014](#)) introduces strong daily aliasing in the resulting Fourier amplitude spectra. More information on the ASAS survey is found in [Pojmanski \(2002\)](#).

#### 2.1.2 The Kilodegree Extremely Little Telescope (KELT)

The Kilodegree Extremely Little Telescope (KELT) survey<sup>2</sup> is an ongoing project that aims at the detection of transiting exoplanets and employs two robotic wide-field telescopes situated at the Winer Observatory in Arizona (KELT-N) and the South African Astronomical Observatory near Sutherland (KELT-S) ([Pepper et al. 2007, 2012](#)). The KELT systems consist of a 4096 x 4096 AP16E Apogee CCD camera (KELT-N) and a 4096 x 4096 Alta U16M Apogee CCD camera (KELT-S) that are used with a Kodak Wratten #8 red-pass filter and either f/1.9 42 mm (wide-angle survey mode; field of view of  $26^\circ.0 \times 26^\circ.0$ ) or f/2.8 200 mm (narrow-angle campaign mode; field of view of  $10^\circ.8 \times 10^\circ.8$ ) Mamiya lenses. The observing cadence is 10 to 30 min. The obtained magnitudes are comparable to standard  $R$  band photometry and useful for stars in the magnitude range from 7 to 13. The time baseline of the KELT data reaches up to 10 years but differs widely from object to object. More information on the KELT survey is found in [Pepper et al. \(2007, 2012\)](#).

#### 2.1.3 The Multi-site All-Sky CAmeRA (MASCARA)

The Multi-site All-Sky CAmeRA (MASCARA)<sup>3</sup> is an ongoing survey run by Leiden University that is dedicated to the

<sup>1</sup> <http://www.astrouw.edu.pl/asas/>

<sup>2</sup> <https://keltsurvey.org/>

<sup>3</sup> <http://mascara1.strw.leidenuniv.nl/>

search for exoplanets around bright stars in the  $V$  magnitude range of 4 to 8 (Talens et al. 2017). MASCARA operates two stations located in the northern hemisphere at the Roque de los Muchachos Observatory, Canary Islands and in the southern hemisphere at La Silla Observatory, Chile, which have been operational since early 2015 and October 2016, respectively. The stations consist of five 4008 x 2672 CCD cameras (northern station: ATIK 11000M; southern station: FLI6 ML11002) equipped with Kodak KAI-11002 interline CCD sensors and f/1.4 24 mm Canon lenses with a 17 mm aperture (field of view per camera of  $53^{\circ}0' \times 74^{\circ}0'$ ). No filters are used, and data are acquired at a cadence of 6.4 s. The currently publicly available data have been binned by 50 points to a cadence of 320 s (Burggraaff et al. 2018). More information on the MASCARA survey can be gleaned from Snellen et al. (2012) and Talens et al. (2017).

## 2.2 Target stars

For the investigation with ASAS-3 and KELT data, a list of mCP stars and mCP star candidates was selected from the most recent version of the Catalogue of Ap, HgMn, and Am stars (Renson & Manfroid 2009, RM09 hereafter). Here, the emphasis was on deriving rotational periods for objects that hitherto lacked this information; therefore, we excluded known ACV variables with well determined rotational periods from further analysis. To this end, the General Catalogue of Variable Stars (Samus et al. 2017), the International Variable Star Index of the AAVSO (VSX; Watson 2006) and the SIMBAD (Wenger et al. 2000) and VizieR (Ochsenbein et al. 2000) databases were queried for classificatory and rotational period information. Suspected or misclassified variables and variables of undetermined type (catalogue-types 'VAR', 'MISC' etc.) were kept. These stars are identified in Table 1 via footnotes that provide essential information from the VSX. 112 mCP stars having ASAS-3 data and 38 mCP stars with KELT data were selected via this approach.

At the time of this writing, MASCARA data were only publicly available for the stars studied by Burggraaff et al. (2018). We crossmatched the light curves published by Burggraaff et al. (2018) with the RM09 catalogue and retrieved data for 144 mCP stars. All of these bright objects are already known as photometric variables with period information of differing quality. Therefore, because of their high quality and cadence, MASCARA data were employed to verify or improve the published periods.

In order to search for rotational variables that might be spectroscopically misclassified mCP stars, we subsequently investigated the remaining objects from the RM09 catalogue (i.e. objects without mCP stars classifications) for which KELT and MASCARA data were available (mainly CP1 and CP3 stars).<sup>4</sup> In this way, 24 stars that show light variability in agreement with rotational modulation were selected and included into the sample as ACV candidates.

## 2.3 Data analysis and classification

The following sections give details on the data processing, the methods used in period analysis and the process of classification.

### 2.3.1 Data processing and period analysis

The light curves of our sample stars were downloaded from the ASAS-3 website, the KELT time series search page on the NASA exoplanet archive<sup>5</sup> and the VizieR catalogue of light curves published by Burggraaff et al. (2018).<sup>6</sup>

Only data sets containing at least 100 measurements were included into the analysis. In the case of ASAS-3 data, no stars brighter than  $V = 7$  mag were investigated to avoid saturation issues. No such issues were identified in the KELT and MASCARA data sets; problematic data sets seem to have been sorted out prior to publication.

In a first step, all data sets were cleaned of outliers by a  $3\sigma$  clipping and searched for periodic signals in the frequency range of  $0 < f(d^{-1}) < 20$  using PERIOD04 (Lenz & Breger 2005). Subsequently, remaining outliers were carefully removed by visual inspection and left-over data points with a quality flag of 'D' ('worst data, probably useless') were removed from the ASAS-3 data sets. No significant instrumental trends were identified in the data for our sample stars.

For a frequency to be deemed significant, it had to show a signal-to-noise (S/N) ratio greater than four ( $SNR > 4$ ). SNR values were determined using PERIOD04. In addition, to avoid spurious detections, all objects with  $4 < SNR < 6$  were required to show a False Alarm Probability (FAP) less than 1% ( $FAP < 0.01$ ). The FAP was calculated using the ANOVA method within the program package PERANSO (Pauzen & Vanmunster 2016). Objects with  $FAP \geq 0.01$  were discarded, except for the star HD 273763. This object shows only weak variability in ASAS-3 data ( $FAP \sim 0.1$ ); however, its light curve is much better defined in data from the All Sky Automated Survey for SuperNovae (ASAS-SN; Shappee et al. 2014), which prove the reality of the light variations.

For the final frequency analysis, the pretreated datasets were again searched for periodic signals in the frequency domain of  $0 < f(d^{-1}) < 5$  with PERIOD04. The resulting phase plots, folded with the most significant frequency, were visually inspected and objects exhibiting convincing phase plots were kept. In all objects, only one significant frequency, its corresponding alias peaks, and, in many cases, harmonics were detected.

Although recent studies based on highly-precise satellite photometry (e.g. Hümmerich et al. 2018) have shown that a considerable fraction of mCP star light curves is more complex than initially thought, most mCP star light curves can be well described by a sine wave and its first harmonic (e.g. North 1984; Mathys & Manfroid 1985; Bernhard et al. 2015a), at least when dealing with ground-based photometry. Therefore, a least-squares fit to the data of all mCP

<sup>4</sup> Because of the ASAS survey's extensive sky coverage, an investigation of non-mCP stars from the RM09 list using ASAS-3 data is a major project that is beyond the scope of the present study.

<sup>5</sup> <https://exoplanetarchive.ipac.caltech.edu/cgi-bin/TblSearch/nph-tblSearchInit?app=ExoTbls&config=kelttimeseries>  
<sup>6</sup> <http://vizier.u-strasbg.fr/viz-bin/VizieR?-source=J/A+A/617/A32>

stars and candidates was performed using PERIOD04 and each light curve was fitted using a Fourier series consisting of the fundamental sine wave and its first harmonic. From this procedure, the semi-amplitudes  $A_1$ ,  $A_2$  and the corresponding phases  $\phi_1$ ,  $\phi_2$  were derived, which are presented with the other results in Section 3.1.

Alias frequencies arise through gaps in the data and the total time span of the data set and are an issue in most ground-based surveys. Aliasing leads to an increased number of high-amplitude peaks in Fourier spectra, thereby rendering the identification of the true period difficult, which must not necessarily show the highest amplitude. This holds especially true for the low-cadence ASAS-3 data, which suffer from strong daily aliasing (cf. Section 2.1.1). To reduce the caveats of aliasing as much as possible, we carefully investigated the spectral windows of the corresponding data sets and double checked the period solution of all doubtful cases. We are confident that we have come up with the correct rotational period – an assumption that is corroborated by the good agreement of our published ASAS-3 period solutions with the literature values (cf. Bernhard et al. 2015b; Hümmelich et al. 2016). Nevertheless, alias periods cannot be excluded from our results based on ASAS-3 data. Because of more favourable observing cadences, this problem is much reduced in KELT and MASCARA data and we do not expect aliasing to be a significant issue here – at least not in the investigated frequency space.

In orientations where two chemical spots come into view during a single rotation cycle, the light curve becomes a double wave (e.g. Maitzen 1980; Jagelka et al. 2019). In the case of spots of similar extent and photometric properties, a symmetric double-wave light curve is to be expected, with ‘maxima’ of approximately the same height. Given data of sufficient precision, it is generally straightforward to identify the true rotational period by a visual inspection of the data folded on the single ( $P$ ) and double ( $2P$ ) periods. However, many of the investigated stars show amplitudes near the detection threshold of the data and a twice longer (or, in some cases, shorter) rotation period cannot be excluded – in particular for objects with significant scatter in their light curves. This applies in particular to objects analyzed with ASAS-3 data. However, symmetric double-wave light curves are comparably rare (they make up 15% of the sample of 650 stars analyzed by Jagelka et al. 2019), so we do not expect this to significantly influence our results.

### 2.3.2 Classification

All stars satisfying the following criteria were classified as ACV variables: (i) a spectral type in agreement with a CP2 or CP4 star classification; (ii) a colour index in rough agreement with the given spectral type [consistency check]; (iii) a period longer than  $P > 0.5$  days; (iv) a variability pattern (shape, amplitude, light curve stability) in agreement with an ACV classification. In all objects, only one significant frequency was found (cf. Section 2.3.1), in agreement with the expectations for ACV variables; no pulsators like e.g. SPB and  $\gamma$  Doradus stars, which generally show multiple periods and quite different frequency spectra from rotating variables, were identified. We will have missed the additional variability seen in roAp stars, which – in addition to rotational light changes – exhibit pulsational variability in the period range

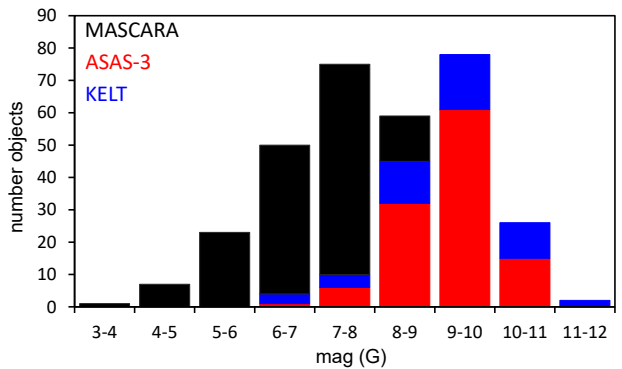


**Figure 1.**  $G$  magnitude histogram of our sample stars. Data sources are represented by different colours.

of about 5 to 20 min (high-overtone, low-degree, and nonradial pulsation modes; Kurtz 1982). This variability, however, is of very small amplitude that is well below the detection limit of the here employed survey data.

Stars of other CP subclasses (mainly CP1 and CP3 stars) and stars from the RM09 catalogue with non-peculiar classifications that show light variability patterns strongly suggestive of rotational modulation have been classified here as ACV candidates. Further (spectroscopic) studies are necessary to decide whether these objects are in fact (i) non-mCP stars showing rotational variability, (ii) spectroscopically misclassified mCP stars or (iii) what other variability mechanisms besides rotational modulation might be at work. These stars are listed in a separate table (Table 3).

We have identified four eclipsing binary stars among our targets (HD 244391, HD 247441, HD 248784 and HD 252519), which, following GCVS standards, have been classified according to light curve shape. These objects are discussed in more detail in Section 3.4.

## 3 RESULTS

### 3.1 Presentation of results

The presentation of results is structured as follows. Table 1 lists essential data for the confirmed mCP stars analyzed with ASAS-3 ( $N = 112$ ) and KELT ( $N = 38$ ) data. With only a very few exceptions that are commented on in the table, these stars are here identified as photometric (and hence ACV) variables for the first time. With more than 150 new rotation periods from newly identified photometric variables or hitherto unidentified/misclassified ACV stars, Table 1 significantly adds to our knowledge of the rotational properties of mCP stars. It is organized as follows:

- Column 1: photometric survey source (ASAS-3 or KELT).
- Column 2: HD number or other conventional identifier.
- Column 3: identification number from RM09.
- Column 4: right ascension (J2000). Positional information was taken from GAIA DR2 (Gaia Collaboration et al. 2016, 2018; Arenou et al. 2018a).
- Column 5: declination (J2000).
- Column 6: Spectral type from RM09; as in this cata-



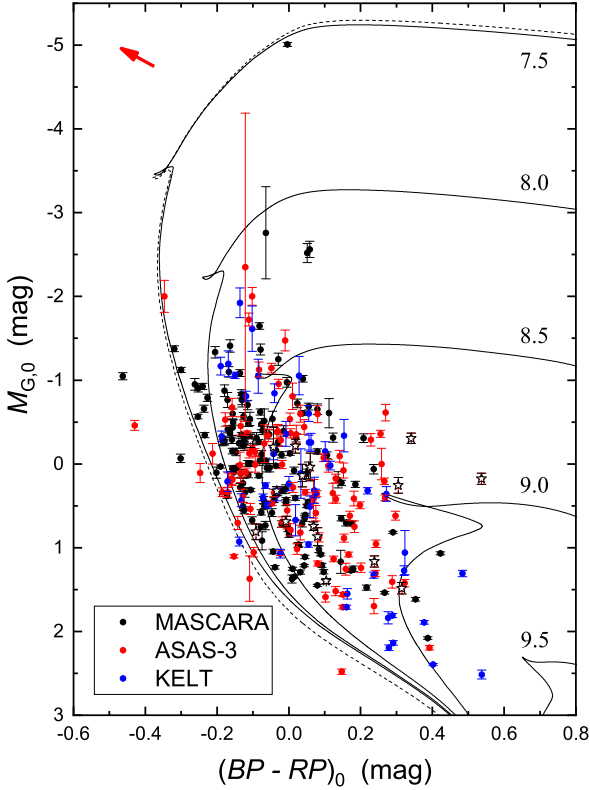


**Figure 2.** The location of our sample stars in the  $(BP - RP)_0$  versus  $M_{G,0}$  diagram. Also shown are PARSEC isochrones for a solar metallicity of  $[Z] = 0.02$  dex (solid lines) and a smaller value of  $[Z] = 0.0152$  dex (dotted line). Logarithmic ages are given. Open asterisks denote stars for which we were not able to derive reddening estimates and adopted zero values. The reddening vector is shown in the upper left corner. Five objects (HD 40146, HD 45530, HD 68419, HD 199122 and HD 273763) are located (within  $3\sigma$ ) below the zero age main sequence. Data sources are represented by different colours.

logue, the ‘p’ denoting peculiarity has been omitted from the spectral classifications.

- Column 7:  $V$  magnitude range.
- Column 8: period (d).
- Column 9: epoch (HJD-2450000); as is standard procedure for ACV variables, time of photometric maximum is indicated.
- Column 10: Semi-amplitude of the fundamental variation ( $A_1$ ).<sup>7</sup>
- Column 11: Semi-amplitude of the first harmonic variation ( $A_2$ ).
- Column 12: Phase of the fundamental variation ( $\phi_1$ ).<sup>8</sup>
- Column 13: Phase of the first harmonic variation ( $\phi_2$ ).
- Column 14:  $G$  mag from GAIA DR2.

<sup>7</sup> Columns 10–13 have only been calculated for ACV variables or candidates.

<sup>8</sup> The calculation of the phase values has been based on the times of observations as provided by the ASAS-3 and KELT databases, i.e. HJD-2450000.

- Column 15:  $(G_{BP} - G_{RP})$  index from GAIA DR2.

Where available, classifications and periods from the VSX are provided in footnotes. Only part of the table is printed here for guidance regarding its form and content. The complete table is given in the Appendix (Table A1).

Known ACV variables whose rotational periods have been investigated with MASCARA data ( $N = 144$ ) are presented in Table 2. It is organized similar to Table 1 but also includes a comparison with the periods listed in the VSX at the time of this writing (June 2019). In the case of strongly discrepant values, the given periods are highlighted in bold font. The complete table is given in the Appendix (Table A2).

Potential rotational variables that were identified among stars of other CP subclasses (mainly CP1 and CP3 stars) or stars from RM09 with non-peculiar classifications are presented here as ACV candidates ( $N = 24$ ) and listed in Table 3. Spectroscopic confirmation of their suspected mCP star status is needed.

The light curves of all objects, folded with the periods listed in Tables A1, A2 and 3 are presented in the Appendix (Section B). The  $G$  magnitude histogram of our sample stars is presented in Fig. 1. It shows a bimodal distribution that illustrates the different data sources used in the analysis, with the ‘bright’ peak corresponding to objects with MASCARA data and the other peak to sources with ASAS-3 and KELT data.

### 3.2 Colour-magnitude diagram

To investigate the astrophysical properties of our sample stars in a colour-magnitude diagram (CMD), we employed the homogeneous Gaia DR2 photometry from Arenou et al. (2018b). Only HD 170000 ( $\phi$  Dra) is not included in this data set because it is too bright. For two stars (HD 122264 and HD 245601), no parallax measurements exist, and two objects (HD 164068 and GSC 2413-00426) have significant negative parallaxes ( $-2.6$  and  $-1.3$  mas, respectively). Because no Hipparcos parallaxes are available (van Leeuwen 2007), we excluded these stars from further analysis. Another object, HD 46462, has a very small parallax (0.08 mas) with a large error (1.09 mas). We strongly suspect that, for some reason we cannot identify, the Gaia DR2 measurement is erroneous and have adopted the Hipparcos satellite parallax of 2.93(52) mas.

For the estimation of the interstellar reddening (absorption), we preferably used the dereddening calibrations in the Strömgren-Crawford system (Pauzen et al. 2005, 2006) valid for mCP stars (Netopil et al. 2008). For 177 stars, all four Strömgren-Crawford indices ( $b - y$ ,  $m_1$ ,  $c_1$  and  $\beta$ ) are available in the catalogue of Pauzen (2015). The transformation of the reddening values was performed using the relations

$$\begin{aligned} A_V &= 1.1A_G = 3.1E(B - V) = 4.3E(b - y) = \\ &= 2.1E(BP - RP). \end{aligned} \quad (1)$$

As next step, the published reddening map by Green et al. (2018) and the individual reddening estimates by Chen et al. (2019) were employed using the distances listed in Bailer-Jones et al. (2018). We note that these references do not cover the entire sky. Therefore, for six-

**Table 1.** Essential data for the mostly new ACV variables analyzed with ASAS-3 and KELT data, sorted by data source and increasing right ascension. The columns denote: (1) Photometric survey source (A=ASAS-3; M=MASCARA; K=KELT). (2) HD number or other conventional identification. (3) Identification number from RM09. (4) Right ascension (J2000; GAIA DR2). (5) Declination (J2000; GAIA DR2). (6) Spectral type from RM09. (7)  $V$  magnitude range. (8) Period, derived in the present investigation. (9) Epoch (HJD-2450000). (10) Semi-amplitude of the fundamental variation ( $A_1$ ). (11) Semi-amplitude of the first harmonic variation ( $A_2$ ). (12) Phase of the fundamental variation ( $\phi_1$ ). (13) Phase of the first harmonic variation ( $\phi_2$ ). (14)  $G$  mag (GAIA DR2). (15) ( $BP - RP$ ) index (GAIA DR2). Where available, classifications and periods from the VSX are provided in footnotes. Only part of the table is printed here for guidance regarding its form and content. The complete table is given in the Appendix (Table A1).

(1) Src	(2) Star	(3) #RM09	(4) $\alpha$ (J2000)	(5) $\delta$ (J2000)	(6) SpT [lit]	(7) $V$ range [mag]	(8) Period [d]	(9) Epoch	(10) $A_1$ [mag]	(11) $A_2$ [mag]	(12) $\phi_1$ [rad]	(13) $\phi_2$ [rad]	(14) $G$ [mag]	(15) ( $BP - RP$ ) [mag]
A	TYC 4701-644-1	3920	02 32 01.69	-03 49 26.9	A0 Sr Eu	10.13-10.15	7.296(4)	3736.63(7)	0.009	0.002	0.496	0.661	10.139	0.273
A	HD 16504	4100	02 35 21.70	-68 09 40.0	B8 Si	9.02-9.03	3.3057(7)	4867.62(3)	0.005	0.002	0.287	0.838	9.021	-0.023
A	HD 25258	6438	04 00 38.96	-04 05 49.6	A2 Sr Eu	10.31-10.33	2.4490(4)	3806.47(2)	0.009	0.001	0.477	0.922	10.304	0.300
A	HD 28365 <sup>a</sup>	7280	04 27 56.40	-13 27 52.3	B9 Si	8.43-8.45	1.80606(9)	4685.91(2)	0.005	0.001	0.245	0.441	8.412	-0.107
A	HD 29925	7690	04 43 00.38	+01 06 28.4	B9 Si	8.32-8.34	0.665558(8)	2558.775(7)	0.007	0.002	0.222	0.624	8.294	-0.107
A	TYC 8510-712-1	8060	04 53 29.13	-53 39 26.4	A0 Si	10.54-10.55	10.263(8)	3652.8(1)	0.005	0.001	0.816	0.044	10.534	-0.092
A	HD 273763	8460	05 05 29.78	-47 53 24.0	A0 Sr	10.96-10.98	0.77418(2)	3430.557(8)	0.008	0.000	0.507	0.814	10.970	0.147
A	HD 36955	9740	05 35 04.54	-01 24 06.6	A2 Cr Eu	9.44-9.45	2.2848(2)	4590.46(2)	0.006	0.002	0.655	0.059	9.416	0.201
A	HD 40146 <sup>b</sup>	10710	05 56 58.90	-03 45 20.4	A0 Si	9.35-9.37	1.78216(8)	3759.68(2)	0.009	0.001	0.168	0.098	9.306	0.250
A	HD 42335 <sup>c</sup>	11290	06 10 05.33	-00 18 08.6	A0 Si	8.40-8.43	5.076(1)	3440.60(5)	0.013	0.004	0.876	0.451	8.358	0.139

<sup>a</sup>NSV 16014 (ACV); <sup>b</sup>ASAS J055659-0345.3 (MISC;  $P_{VSX} = 1.781649$  d); <sup>c</sup>HIP 29253 (VAR;  $P_{VSX} = 5.07872$  d)

**Table 2.** Essential data for the known ACV variables whose rotational periods were investigated with MASCARA data, sorted by increasing right ascension. The columns denote: (1) HD number or other conventional identification. (2) Identification number from RM09. (3) Right ascension (J2000; GAIA DR2). (4) Declination (J2000; GAIA DR2). (5) Spectral type from RM09. (6)  $V$  magnitude range. (7) Literature period (VSX). (8) Period (this work). (9) Epoch (HJD-2450000). (10) Semi-amplitude of the fundamental variation ( $A_1$ ). (11) Semi-amplitude of the first harmonic variation ( $A_2$ ). (12) Phase of the fundamental variation ( $\phi_1$ ). (13) Phase of the first harmonic variation ( $\phi_2$ ). (14)  $G$  mag (GAIA DR2). (15) ( $BP - RP$ ) index (GAIA DR2). Only part of the table is printed here for guidance regarding its form and content. The complete table is given in the Appendix (Table A2).

(1) Star	(2) #RM09	(3) $\alpha$ (J2000)	(4) $\delta$ (J2000)	(5) SpT [lit]	(6) $V$ range [mag]	(7) $P_{VSX}$ [d]	(8) $P_{MASCARA}$ [d]	(9) Epoch	(10) $A_1$ [mag]	(11) $A_2$ [mag]	(12) $\phi_1$ [rad]	(13) $\phi_2$ [rad]	(14) $G$ [mag]	(15) ( $BP - RP$ ) [mag]
HD 3580	970	00 38 31.86	-20 17 47.6	B8 Si	6.71-6.73	1.4788	1.47561(4)	7219.71(1)	0.006	0.001	0.986	0.484	6.687	-0.157
HD 4778	1250	00 50 18.27	+45 00 08.2	A1 Cr Sr Eu	6.10-6.13	2.5481	2.5619(1)	7185.70(2)	0.006	0.008	0.899	0.974	6.110	0.028
HD 4796	1263	00 52 28.98	+79 50 25.6	A0 Sr Si	7.71-7.73	8	7.987(2)	7060.62(7)	0.009	0.000	0.765	0.323	7.695	0.152
HD 7676	1880	01 16 06.81	-34 08 55.8	A5 Sr Cr Eu	8.36-8.41	5.0976	5.088(2)	7252.84(5)	0.022	0.007	0.010	0.744	8.388	0.217
HD 7546	1870	01 16 24.50	+48 04 56.1	B8 Si	6.60-6.62	5.229	5.4060(9)	7057.38(5)	0.009	0.004	0.250	0.826	6.563	-0.002
HD 8441	2050	01 24 18.69	+43 08 31.6	A2 Sr	6.66-6.68	69.92	69.9(1)	7230.2(7)	0.009	0.004	0.228	0.942	6.651	0.079
HD 10221	2550	01 42 20.51	+68 02 34.9	A0 Si Sr Cr	5.54-5.58	3.1848	3.1528(2)	7216.49(3)	0.017	0.005	0.769	0.899	5.529	-0.064
HD 10783	2670	01 45 42.52	+08 33 33.2	A2 Si Cr Sr	6.53-6.56	4.1321	4.1335(3)	7057.30(4)	0.009	0.005	0.374	0.063	6.514	-0.009
HD 11415	2870	01 54 23.74	+63 40 12.4	B3 He wk.	3.34-3.35	<b>0.08946</b>	<b>14.53(1)</b>	7192.6(1)	0.006	0.002	0.528	0.503	3.261	0.070
HD 12288	3130	02 03 30.49	+69 34 56.4	A2 Cr Si	7.72-7.74	34.9	35.73(3)	7218.6(3)	0.007	0.002	0.772	0.633	7.706	0.177

teen objects (HD 71006, HD 88701, HD 98956, HD 111672, HD 129189, HD 147174, HD 162306, HD 162639, HD 163583, HD 167024, HD 168108, HD 172626, HD 193382, TYC 7415-2499-1, TYC 8143-3244-1 and TYC 8510-712-1), we were not able to derive reddening estimates and have thus adopted zero values.

In Fig. 2, we present the CMD of our sample stars together with PARSEC isochrones (Bressan et al. 2012) for a solar metallicity of  $[Z]=0.02$  dex. We favour this value because it has been shown to be consistent with recent results of helioseismology (Vagnozzi 2019). Adopting a smaller value, as e.g. suggested by Bressan et al. (2012), shifts the main sequence slightly to the blue, as indicated in Figure 2. In general, our reddening estimates seem to be very reliable. However, five objects (HD 40146, HD 45530, HD 68419, HD 199122 and HD 273763) are located within  $3\sigma$  below the zero-age main sequence (ZAMS). On the basis of Strömgren-Crawford photometry, which generally is very reliable, we derive absorption values ( $A_G$ ) between 0.45 and 0.64 mag

for HD 45530, HD 68419 and HD 199122. In the case of HD 40146, we derived a value of 1.31 mag based on reddening maps. This star is a member of the Orion OB1 association (Romanyuk et al. 2013) and hence situated in a part of the sky where strong differential reddening is evident which might cause an overestimation. HD 273763, on the other hand, seems to exhibit no reddening at all, which is to be expected considering its location at a Galactic latitude of  $-37^\circ$ . Interestingly, it is a high proper-motion star (Tetzlaff et al. 2011). Otherwise, no indications of measurement errors or false identifications were found. Two further stars (HD 91590 and TYC 6545-2278-1) are situated below the ZAMS in Fig. 2 but do not satisfy the  $3\sigma$  criterion.

From the distribution of stars in Fig. 2, we find that almost all objects are between 100 Myr and 1 Gyr old, with an apparent lack of very young stars (pertaining, in particular, to objects with absolute magnitudes below 1.5 mag). This is in agreement with the currently favoured model predictions that almost all mCP stars are hydrogen

**Table 3.** Essential data for the ACV variable candidates identified among stars of other CP subclasses or stars from RM09 with non-peculiar classifications, sorted by increasing right ascension. The columns denote: (1) Data source. (2) HD number or other conventional identification. (3) Identification number from RM09. (4) Right ascension (J2000; GAIA DR2). (5) Declination (J2000; GAIA DR2). (6) Spectral type from RM09. (7)  $V$  magnitude range. (8) Period, derived in the present investigation. (9) Epoch (HJD-2450000). (10) Semi-amplitude of the fundamental variation ( $A_1$ ). (11) Semi-amplitude of the first harmonic variation ( $A_2$ ). (12) Phase of the fundamental variation ( $\phi_1$ ). (13) Phase of the first harmonic variation ( $\phi_2$ ). (14)  $G$  mag (GAIA DR2). (15) ( $G_{BP} - G_{RP}$ ) index (GAIA DR2).

(1) Source	(2) Star	(3) ID (RM09)	(4) $\alpha$ (J2000)	(5) $\delta$ (J2000)	(6) SpT [lit]	(7) Range (V) [mag]	(8) Period [d]	(9) Epoch [HJD-2450000]	(10) $A_1$ [mag]	(11) $A_2$ [mag]	(12) $\phi_1$ [rad]	(13) $\phi_2$ [rad]	(14) $G$ [mag]	(15) $(G_{BP} - G_{RP})$ [mag]
MASCARA	HD 17157	1795	01 13 09.78	+61 42 22.3	B9	6.43-6.46	1.00674(2)	7151.70(1)	0.015	0.001	0.944	0.389	6.477	-0.004
KELT	TYC 2903-775-1	8178	05 02 37.13	+42 33 16.4	A2	10.86-10.87	3.2402(2)	4057.84(3)	0.007	0.001	0.396	0.411	10.828	0.346
KELT	HD 36589 <sup>a</sup>	9520	05 33 38.84	+20 28 27.2	B7 HgMn?	6.18-6.19	7.656(2)	4057.77(7)	0.003	0.001	0.836	0.471	6.156	-0.006
KELT	TYC 2412-1315-1	10035	05 39 53.12	+34 31 27.2	A0-	8.74-8.76	0.75402(2)	4038.903(7)	0.007	0.000	0.258	0.912	8.663	0.426
KELT	HD 247209	10315	05 46 12.12	+31 23 16.0	B9-	9.33-9.35	5.710(1)	4379.99(5)	0.007	0.002	0.674	0.837	9.314	0.106
KELT	HD 250237	10859	06 01 21.03	+32 57 50.0	A0-	9.98-9.99	2.6873(2)	4035.81(2)	0.004	0.001	0.064	0.954	9.960	0.340
MASCARA	HD 55667	15134	07 21 50.63	+75 05 22.0	A2	6.93-6.96	1.79690(6)	7176.49(1)	0.014	0.003	0.936	0.077	6.938	0.024
MASCARA	HD 101753	29335	11 42 44.02	+18 14 31.3	B9	7.35-7.41	7.828(1)	7056.80(7)	0.029	0.006	0.304	0.679	7.371	-0.184
MASCARA	HD 180582	50098	19 15 17.24	+40 06 49.2	B9	8.07-8.15	2.2908(1)	7085.66(2)	0.035	0.017	0.452	0.590	8.092	-0.129
MASCARA	HD 182865	50555	19 25 39.02	+26 06 14.3	B8	7.36-7.38	6.424(1)	7079.50(6)	0.012	0.003	0.693	0.300	7.304	0.219
MASCARA	HD 183142	50623	19 26 01.21	+45 00 47.1	B8	7.04-7.09	1.08805(2)	7064.78(1)	0.022	0.001	0.698	0.067	7.034	-0.221
MASCARA	HD 189775	52618	19 59 15.36	+52 03 20.6	B5	6.09-6.15	2.6074(1)	7135.63(2)	0.028	0.003	0.049	0.511	6.097	-0.239
MASCARA	HD 193553	54027	20 19 49.81	+29 43 36.8	B8	6.75-6.79	6.8197(9)	7076.68(6)	0.019	0.003	0.023	0.520	6.733	-0.190
MASCARA	HD 195447	54447	20 29 20.82	+50 27 37.2	B9	7.56-7.59	5.3970(6)	7060.57(5)	0.014	0.005	0.501	0.282	7.557	0.072
KELT	HD 196655	54880	20 37 50.18	+29 43 17.9	A2-	8.24-8.25	2.3409(2)	4274.80(2)	0.005	0.000	0.606	0.133	8.214	0.145
MASCARA	HD 199122	55433	20 53 39.89	+41 02 58.4	A2	7.56-7.60	1.24673(3)	7085.78(1)	0.024	0.001	0.261	0.091	7.575	-0.130
KELT	TYC 3171-971-1	55450	20 54 03.30	+40 42 23.8	A4-	8.75-8.76	1.46591(5)	4276.93(1)	0.002	0.000	0.208	0.306	8.714	0.366
KELT	HD 200407 <sup>b</sup>	55840	21 01 47.46	+44 11 12.9	A4-F1	6.75-6.76	8.325(3)	4386.60(8)	0.004	0.001	0.833	0.369	6.686	0.418
KELT	TYC 2709-59-1	56010	21 05 11.27	+34 40 49.1	A5-	9.31-9.32	2.4770(2)	4274.89(2)	0.006	0.001	0.962	0.062	9.264	0.322
MASCARA	HD 204374	56913	21 26 28.36	+49 16 49.0	A0	7.92-7.99	1.27985(2)	7151.68(1)	0.030	0.005	0.886	0.787	7.917	-0.116
KELT	HD 204936	57090	21 31 20.66	+21 12 16.2	A2-	8.54-8.55	13.56(1)	4601.9(1)	0.004	0.003	0.401	0.263	8.437	0.512
KELT	TYC 2712-2178-1	57270	21 35 16.02	+33 58 31.6	A2-	9.48-9.49	0.56069(1)	4260.906(5)	0.003	0.000	0.422	0.740	9.419	0.493
MASCARA	HD 217062	59915	22 56 56.13	+59 57 42.2	B9	7.19-7.23	1.26737(3)	7176.69(1)	0.021	0.000	0.078	0.596	7.192	-0.073
MASCARA	HD 220885	60550	23 27 07.39	+42 54 43.2	B9 Mn	5.72-5.76	1.47905(4)	7056.34(1)	0.016	0.005	0.856	0.135	5.728	-0.002

<sup>a</sup> NSV 2132; suspected of variability by Crawford (1963); non-variable according to the VSX.

<sup>b</sup> NSV 25432; possible microvariable according to Rufener (1981); range is 6.74-6.76 mag (V) according to the VSX.

burning main-sequence objects. Bagnulo et al. (2006) and Landstreet et al. (2007, 2008) have shown that the magnetic field at the surface of mCP stars decreases with time because of magnetic flux conversation with increased stellar radius and additional decay (cf. also Fossati et al. 2016; Shultz et al. 2019). The time scales involved vary strongly with mass ( $\sim 250$  Myr for stars of  $2-3 M_{\odot}$  to  $\sim 15$  Myr for stars of  $4-5 M_{\odot}$  according to Landstreet et al. 2008). The more evolved stars of our sample (see below) may provide an interesting testbed to further elaborate on these findings.

Landstreet et al. (2007) find magnetic fields in mCP stars from the ZAMS to the terminal-age main sequence (TAMS). The assumption that the magnetic fields are already there at late stages of the pre-main sequence phase has been substantiated by the discovery of global fields in Herbig Ae/Be stars (e.g. Wade et al. 2005; Alecian et al. 2013). In contrast to this, as regards our sample stars, we find a conspicuous lack of mCP stars directly on the ZAMS, which seems to imply that a certain amount of time is necessary either for the magnetic field to build up in strength or for the peculiarities to develop. This recalls the observations of Hubrig et al. (2000), who find that mCP stars with  $M_{\odot} \leq 3$  are typically more than 30% of the way through their life on the main sequence. The assumption that the magnetic fields appear only after a certain time, however, is in contrast with theoretical considerations that have narrowed down the time a fossil field requires to relax onto a stable configuration to just a few Alfvén times (Braithwaite & Nordlund 2006) and has been disputed by several studies (cf. the discussion in Landstreet et al. 2007). Our study does not follow the methodological approach of Hubrig et al. (2000) and therefore cannot be affected by the same systematic issues. We further cannot identify systematic errors in our treatment of the data that have led to the construction of Fig. 2, such

as a possible overestimation of the luminosity of our sample stars. In summary, with the currently available data, we are unable to satisfactorily explain and assess our observation.

Several stars of our sample seem to have already left the main sequence and are situated on the subgiant branch – albeit well before the first dredge-up (Vassiliadis & Wood 1993). In these evolutionary stages, diffusion seems to only play a minor role in the stellar atmospheres of intermediate mass stars. Bailey et al. (2014) have shown that several elements, such as the iron-peak elements Cr, Fe and Ti, decrease in abundance with age, approaching near-solar values close to the terminal-age main sequence, while the abundance of He increases. In this respect, it would be highly interesting to investigate the abundance patterns of the more evolved mCP stars in our sample.

### 3.3 Rotational periods

Fig. 3 shows a histogram of the period distribution of the 294 confirmed mCP stars of our sample. The rotational period distribution is in very good agreement with the literature (e.g. Renson & Manfroid 2009; Netopil et al. 2017) and shows the typical peak distribution in the  $0.0 < \log(P[d]) < 0.5$  bin. We note that because of the time span and characteristics of the here employed photometric time-series data, we will have missed very slowly rotating ACV variables with periods of several years or more (Mathys 2017).

As has been pointed out (Section 2.2), at the time of this writing, MASCARA data were only publicly available for known variables with period information of differing quality. These data were therefore employed to verify or improve the published periods. A comparison of the VSX periods with the periods derived from the analysis of MASCARA data in

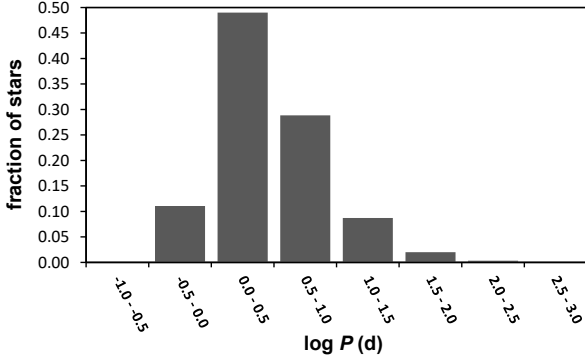


**Figure 3.** Rotational period histogram of the 294 confirmed mCP stars of our sample.

the present work is presented in the upper panel of Fig. 4; the lower panel illustrates the corresponding  $\delta P$  value histogram. The agreement is generally very good, highlighting the quality of the VSX period data which – although based on very different sources – are constantly being updated with new results from the literature. Only for some objects, the discrepancy between the VSX and MASCARA periods is striking. The observed differences are most likely due to alias periods, as e.g. in the case of HD 193722 ( $P_{\text{VSX}} = 1.132854$  d vs.  $P_{\text{MASCARA}} = 8.530(1)$  d), or overinterpretation of short or sparsely sampled datasets.

It is well known that some ACV variables show variations of the rotational (photometric) period over time (Mikulášek et al. 2017). However, no detailed analysis of this phenomenon has been carried out for a statistically sound sample of stars. The four ACVs variables with the currently largest known period variations – HD 37479 (He strong star; Townsend et al. 2010; Oksala et al. 2012), HD 37776 (He strong star; Mikulášek et al. 2011), HD 124224 (classical Si star; Smith et al. 1997; Pyper et al. 1998) and HD 125630 (cool SrCrEu star; Mikulášek et al. 2015) – form a very heterogeneous sample of mCP stars. However, the observed period changes range from 0.08 to almost  $3 \text{ s yr}^{-1}$ , which equals to about  $9 \times 10^{-8} \text{ d}^{-1}$ . This is well below the accuracy of the derived periods (Tables 1 and 2). Therefore, the possible occurrence of period changes in our sample stars are not expected to account for even the slight discrepancies between the (mostly older) VSX periods and the here derived periods.

### 3.4 Eclipsing binary systems

This sections contains a short discussion of the eclipsing binary systems identified among our sample stars.

#### 3.4.1 HD 244391

HD 244391 is listed with a spectral type of B8pSiSr in the RM09 catalogue. Only five references to this star are contained in the SIMBAD database; the only photometric study available is that of Wraight et al. (2012), who investigated mCP stars with the STEREO satellite and found HD 244391 to be constant.

KELT data clearly indicate that the star is an eclipsing

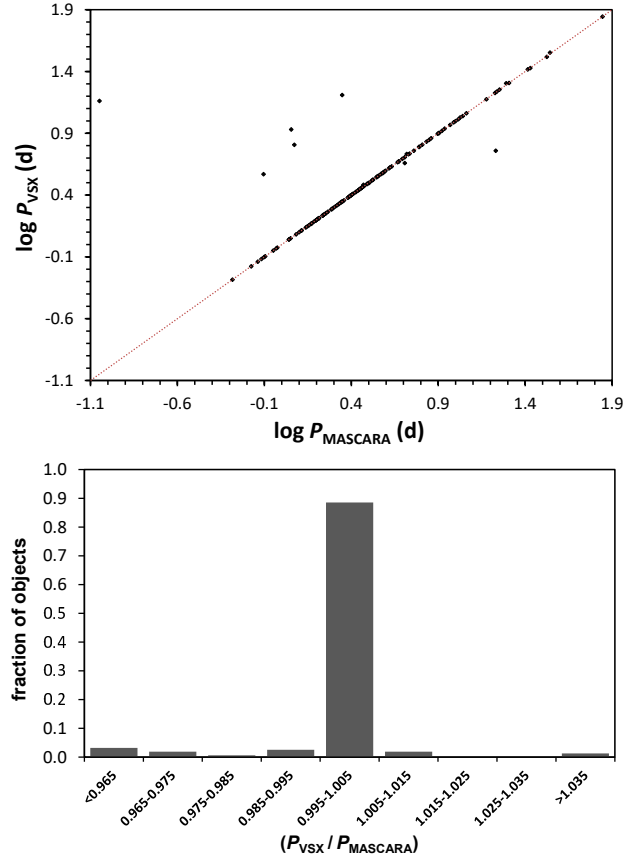


**Figure 4.** The upper panel shows a comparison of the VSX periods and the periods derived from the analysis of MASCARA data in the present work. The lower panel gives the corresponding  $\delta P$  value histogram.

binary with a period of  $P = 6.0783(4)$  d. The primary minimum is sharp and suggests a detached or semi-detached system (cf. Figure 5); a secondary eclipse is visible at phase  $\varphi = 0.5$ . No secondary variability due to ACV-type rotational variability of one (or both) components could be identified.

mCP stars are very rarely found in close binary systems, in particular eclipsing ones (Niemczura et al. 2017; Kochukhov et al. 2018); if proven that at least one component of this system is indeed a CP2 star, as suggested by the spectral type, HD 244391 would be an object of high interest. We therefore strongly encourage spectroscopic and spectropolarimetric studies to shed more light on the nature of the HD 244391 system.

#### 3.4.2 HD 247441

HD 247441 was identified as an eclipsing binary system by Wraight et al. (2011), who derived a period of  $P = 4.26760$  d from STEREO data and listed a spectral type of A0, which was gleaned from the SIMBAD database and obviously goes back to Cannon (1931). Newer spectroscopic studies, however, have suggested the presence of chemical peculiarities, and the star is listed with a spectral type of B9pSiSr in the RM09 catalogue. Other than that, not much is known about HD 247441, to which the SIMBAD database lists only four references.



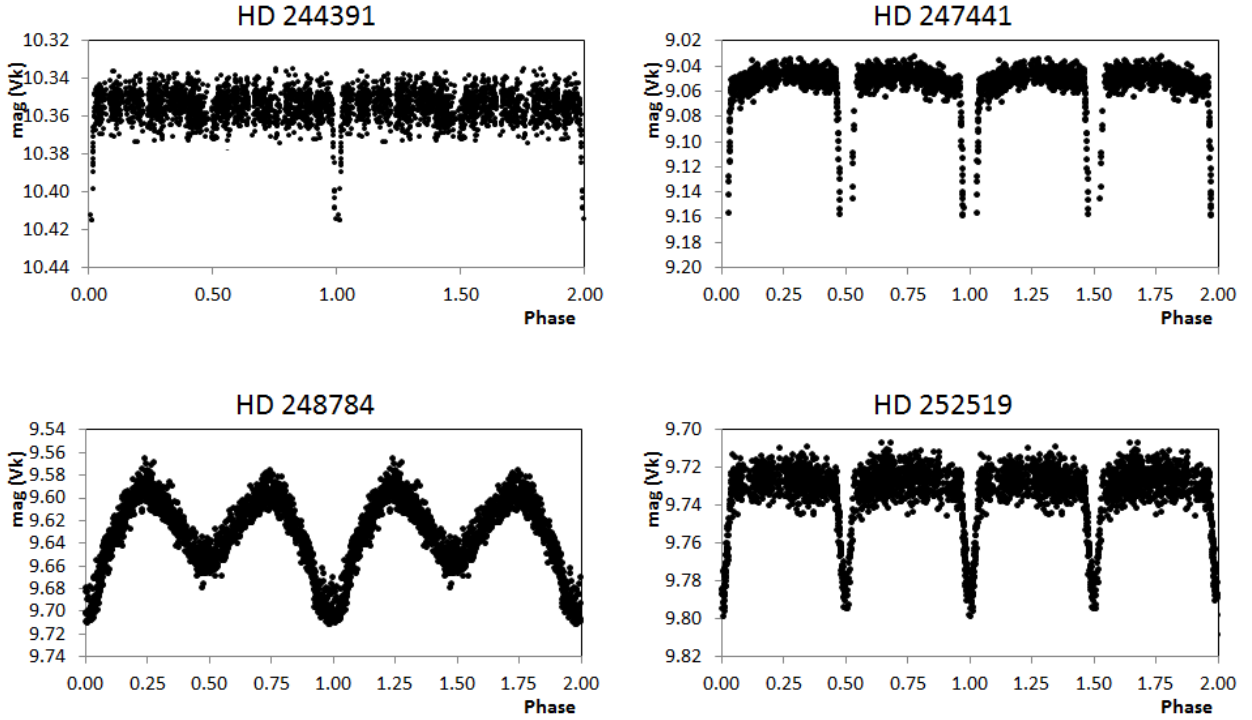


**Figure 5.** The KELT light curves of the eclipsing binaries HD 244391, HD 247441, HD 248784 and HD 252519, folded on the orbital periods of, respectively,  $P_{\text{orb}} = 6.0783(4)$  d,  $P_{\text{orb}} = 4.26756(5)$  d,  $P_{\text{orb}} = 0.81821(1)$  d and  $P_{\text{orb}} = 3.07948(2)$  d.

Employing KELT data, we have derived an orbital period of  $P = 4.26756(5)$  d, in agreement with the results of [Wraight et al. \(2011\)](#). The light curve of the star is shown in Fig. 5. No additional variability due to rotational variability of one (or both) components could be identified. We nevertheless consider HD 247441 another good candidate for an eclipsing system containing an *mCP* star and encourage further studies.

#### 3.4.3 HD 248784

HD 248784 is identified here as a photometric variable for the first time. No detailed studies of this object exist, to which only two references are listed in the SIMBAD database. The star's KELT light curve resembles a close binary system showing proximity effects (Fig. 5), which is in agreement with the rather short photometric period of  $P = 0.81821(1)$  d that we identify with the orbital period. Although certain spot configurations can lead to similar light curves in ACV variables (cf. the light curves of our sample stars shown in Section B), the large amplitude ( $\sim 0.11$  mag) and the rather sharp primary minimum are strongly suggestive of an eclipsing binary system. No secondary variability is present in the light curve.

The star is listed with a spectral type of B8pSiSr in the RM09 catalogue and we encourage spectroscopic studies to investigate the presence of an *mCP* star component in the HD 248784 system.

#### 3.4.4 HD 252519

In their variability study of TESS input catalogue sources with KELT data, [Oelkers et al. \(2018\)](#) classified HD 252519 as non-variable. No other studies of this star exist, to which the SIMBAD database contains only two references. However, on the basis of the same data that [Oelkers et al. \(2018\)](#) used, we clearly find that the star is an eclipsing binary system and identify an orbital period of  $P = 3.07948(2)$  d. Thus, the star is presented here as a photometric variable for the first time. It is listed with a spectral type of A1pCrSi in the RM09 catalogue.

The light curve of HD 252519 is typical of a detached or semi-detached system (cf. Figure 5) and shows a secondary eclipse at phase  $\varphi = 0.5$ . We could identify no secondary variability due to the possible presence of a rotationally variable *mCP* star in the system.

The star has been observed two times with the Large Sky Area Multi-Object Fiber Spectroscopic Telescope (LAMOST; [Zhao et al. 2012](#); [Cui et al. 2012](#)). We have downloaded the spectra in their DR4 reduction via the VizieR service. They are shown in Figure 6, together with a synthetic spectrum which was computed using the program SPECTRUM<sup>9</sup> ([Gray & Corbally 1994](#)) and an ATLAS9 model atmosphere ([Castelli & Kurucz 2003](#)) for  $T_{\text{eff}} = 8750$  K,  $\log g = 4.0$ ,  $[M/H] = 0.0$  and a microturbulent velocity of 2 km/s. The output spectrum was smoothed to a resolution of  $4 \text{ \AA}$  and an output spacing of  $1 \text{ \AA}$  to match the LAMOST resolution.

<sup>9</sup> <http://www.appstate.edu/~grayro/spectrum/spectrum.html>

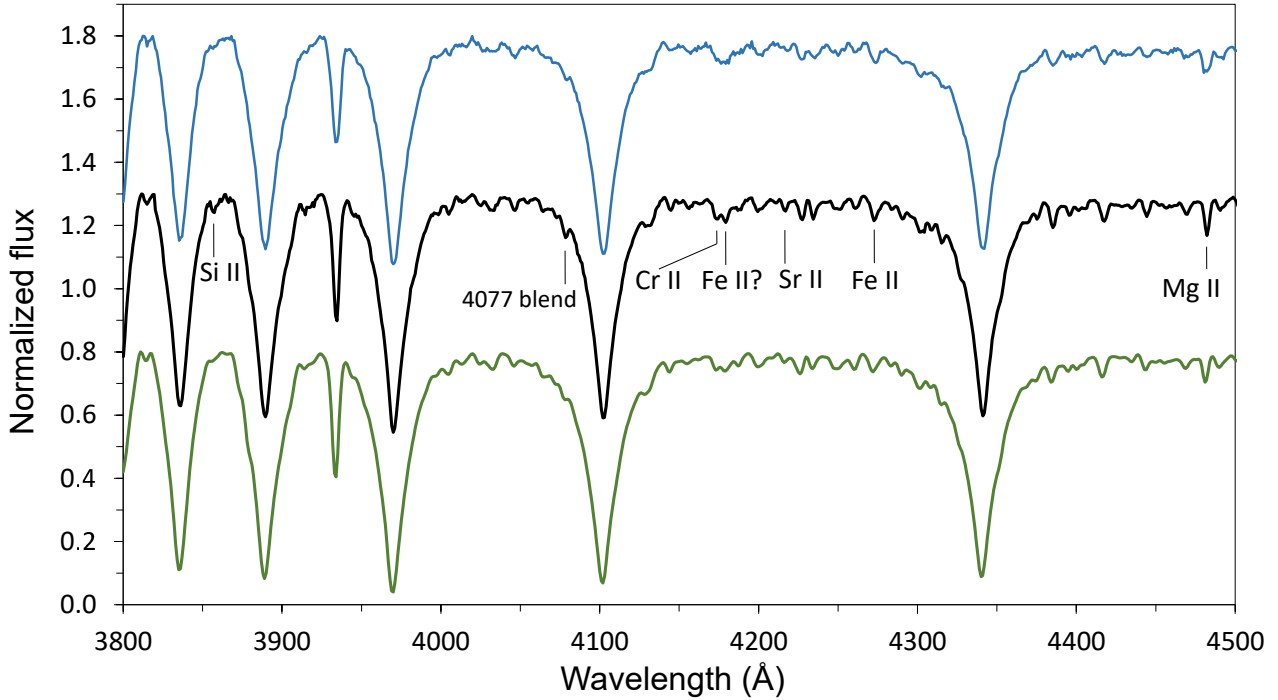


**Figure 6.** A comparison of the LAMOST DR4 spectra of HD 252519 taken on 5 January 2012 (*'spectrum1'*: upper spectrum, blue) and 9 January 2014 (*'spectrum2'*: middle spectrum, black) to a synthetic spectrum with  $T_{\text{eff}} = 8750$  K,  $\log g = 4.0$ ,  $[M/H] = 0.0$  and a microturbulent velocity of 2 km/s (lower spectrum, green). Only the blue-violet spectral region is shown. Some lines of interest are indicated.

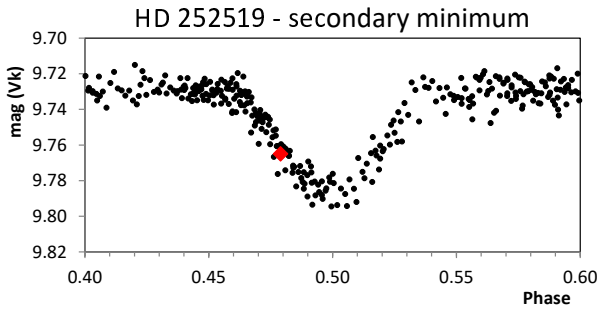


**Figure 7.** A zoom-in on the secondary minimum of the eclipsing binary HD 252519, based on KELT data. The orbital period is  $P = 3.07948(2)$  d. The red dot marks the orbital phase during which the second LAMOST spectrum (*'spectrum2'*) was acquired (JD 2455932.1895).

The first LAMOST spectrum (upper spectrum, blue; *spectrum1* hereafter) was taken on 5 January 2012 at a JD of 2455932.1895 (S/N of  $g$  filter = 249), which corresponds to an orbital phase of  $\phi = 0.818$ . The second LAMOST spectrum (middle spectrum, black; *spectrum2* hereafter) was taken on 9 January 2014 at a JD of 2456667.1430 (S/N of  $g$  filter = 712), which corresponds to an orbital phase of  $\phi = 0.479$ ; hence, it was acquired during the secondary minimum.

*Spectrum1* is well fitted with the shown synthetic spectrum (lower spectrum, green), whose parameters correspond to a main sequence object of spectral type A2. The hydrogen

line profiles match perfectly; however, the observed Ca II K line in HD 252519 appears slightly weak. We nevertheless derive a spectral type of A2V. From the derived orbital phase, we conclude that *spectrum1* belongs to the primary star of the system, although there is a contribution of unknown strength from the secondary component.

*Spectrum2*, which was taken during the secondary minimum (cf. Fig. 7) and is therefore dominated by light from the secondary star, looks superficially similar but exhibits some significant differences. The Ca II K line perfectly matches that of an A2V star; the hydrogen line profile points to a slightly later type (A3V). We hence derive a spectral type of A2.5V from the available spectrum. Furthermore, we identify a minor strengthening of the absorption lines at 3856 Å (Si II), 4077 Å (Si II? Cr II? Sr II?), 4172 Å (Cr II), 4179 Å (Fe II?), 4216 Å (Sr II), 4233 Å (Fe II) and 4281 Å (Mg II). This is well in line with a CP2 star classification and the RM09 spectral type of A1pCrSi and strong evidence that the system of HD 252519 indeed harbours an mCP star component, thus rendering it a potentially most interesting object (cf. Kochukhov et al. 2018). Further, detailed studies of this interesting object are strongly encouraged.

#### 4 CONCLUSION

Archival photometric time-series data from the ASAS-3, KELT and MASCARA surveys were employed to improve existing rotational period information and derive new rotational periods for mCP stars hitherto lacking this informa-

tion. Our final sample consists of 294 mCP stars, a considerable amount of which (more than 40%) are here presented as variable stars for the first time. In addition, 24 mCP star candidates have been identified that show light variability in agreement with rotational modulation but lack spectroscopic confirmation.

Summary data and folded light curves are presented for all objects. From an investigation of our sample stars in the colour-magnitude diagram, we conclude that the vast majority of our sample stars are between 100 Myr and 1 Gyr old. We find a conspicuous lack of mCP stars directly on the zero age main sequence; several stars of our sample seem to have left the main sequence and are situated on the subgiant branch, albeit well before the first dredge-up. Our results are in agreement with the currently-favoured model predictions that, except for rare cases, mCP stars are hydrogen burning main-sequence objects.

The rotational period distribution of our sample stars is typical of ACV variables and agrees well with results from the literature. Our sample significantly enhances the sample size of mCP stars with accurate rotational period information and facilitates further research into the rotational properties of mCP stars and their evolution in time.

Four eclipsing binary systems have been identified among our sample stars (HD 244391, HD 247441, HD 248784 and HD 252519). As mCP stars are very rarely found in close binary systems – in particular eclipsing ones –, these objects are potentially of great interest. Using archival LAMOST spectra, we find strong evidence that the system of HD 252519 indeed harbours an mCP star component. All systems should be investigated with time-resolved spectroscopy for confirmation.

## ACKNOWLEDGEMENTS

We thank the anonymous referee for the thoughtful report that helped to improve the paper. Some of the data presented in this paper were obtained from the Mikulski Archive for Space Telescopes (MAST). STScI is operated by the Association of Universities for Research in Astronomy, Inc., under NASA contract NAS5-26555. Support for MAST for non-HST data is provided by the NASA Office of Space Science via grant NNX09AF08G and by other grants and contracts. Guoshoujing Telescope (the Large Sky Area Multi-Object Fiber Spectroscopic Telescope LAMOST) is a National Major Scientific Project built by the Chinese Academy of Sciences. Funding for the project has been provided by the National Development and Reform Commission. LAMOST is operated and managed by the National Astronomical Observatories, Chinese Academy of Sciences. This research has made use of the VizieR catalogue access tool (DOI: 10.26093/cds/vizieR) and the SIMBAD database, both operated at CDS, Strasbourg, France.

## REFERENCES

Alecian E., et al., 2013, *MNRAS*, **429**, 1001  
 Arenou F., et al., 2018a, *A&A*, **616**, A17  
 Arenou F., et al., 2018b, *A&A*, **616**, A17  
 Aurière M., et al., 2007, *A&A*, **475**, 1053

Bagnulo S., Landstreet J. D., Mason E., Andretta V., Silaj J., Wade G. A., 2006, *A&A*, **450**, 777  
 Bailer-Jones C. A. L., Rybizki J., Foesneau M., Mantelet G., Andrae R., 2018, *AJ*, **156**, 58  
 Bailey J. D., Landstreet J. D., Bagnulo S., 2014, *A&A*, **561**, A147  
 Bernhard K., Hümmerich S., Paunzen E., 2015a, *Astronomische Nachrichten*, **336**, 981  
 Bernhard K., Hümmerich S., Otero S., Paunzen E., 2015b, *A&A*, **581**, A138  
 Bowman D. M., Buysschaert B., Neiner C., Pápics P. I., Oksala M. E., Aerts C., 2018, *A&A*, **616**, A77  
 Braithwaite J., Nordlund Å., 2006, *A&A*, **450**, 1077  
 Bressan A., Marigo P., Girardi L., Salasnich B., Dal Cero C., Rubele S., Nanni A., 2012, *MNRAS*, **427**, 127  
 Burggraaf O., et al., 2018, *A&A*, **617**, A32  
 Cannon A. J., 1931, *Annals of Harvard College Observatory*, **100**, 61  
 Castelli F., Kurucz R. L., 2003, in Piskunov N., Weiss W. W., Gray D. F., eds, *IAU Symposium Vol. 210, Modelling of Stellar Atmospheres*. p. A20 ([arXiv:astro-ph/0405087](https://arxiv.org/abs/astro-ph/0405087))  
 Chen B. Q., et al., 2019, *MNRAS*, **483**, 4277  
 Crawford D. L., 1963, *ApJ*, **137**, 530  
 Cui X.-Q., et al., 2012, *Research in Astronomy and Astrophysics*, **12**, 1197  
 David-Uraz A., et al., 2019, *MNRAS*, p. 1133  
 Fossati L., et al., 2016, *A&A*, **592**, A84  
 Gaia Collaboration et al., 2016, *A&A*, **595**, A1  
 Gaia Collaboration et al., 2018, *A&A*, **616**, A1  
 Ghazaryan S., Alecian G., Hakobyan A. A., 2018, *MNRAS*, **480**, 2953  
 Gray R. O., Corbally C. J., 1994, *AJ*, **107**, 742  
 Gray R. O., Corbally J. C., 2009, *Stellar Spectral Classification*  
 Green G. M., et al., 2018, *MNRAS*, **478**, 651  
 Hubrig S., North P., Mathys G., 2000, *ApJ*, **539**, 352  
 Hümmerich S., Paunzen E., Bernhard K., 2016, *AJ*, **152**, 104  
 Hümmerich S., et al., 2018, *A&A*, **619**, A98  
 Jagelka M., Mikulášek Z., Hümmerich S., Paunzen E., 2019, *A&A*, **622**, A199  
 Kochukhov O., Johnston C., Alecian E., Wade G. A., 2018, *MNRAS*, **478**, 1749  
 Kurtz D. W., 1982, *MNRAS*, **200**, 807  
 Landstreet J. D., Bagnulo S., Andretta V., Fossati L., Mason E., Silaj J., Wade G. A., 2007, *A&A*, **470**, 685  
 Landstreet J. D., et al., 2008, *A&A*, **481**, 465  
 Lanz T., Artru M. C., Le Dourneuf M., Hubeny I., 1996, *A&A*, **309**, 218  
 Lenz P., Breger M., 2005, *Communications in Asteroseismology*, **146**, 53  
 Maitzen H. M., 1980, *A&A*, **89**, 230  
 Maitzen H. M., 1984, *A&A*, **138**, 493  
 Mathys G., 2017, *A&A*, **601**, A14  
 Mathys G., Manfroid J., 1985, *A&AS*, **60**, 17  
 Michaud G., 1970, *ApJ*, **160**, 641  
 Mikulášek Z., et al., 2011, *A&A*, **534**, L5  
 Mikulášek Z., Jan'ik J., Krčička J., Zejda M., Jagelka M., 2015, *Preliminary Study of the Moderately Cool Chemically Peculiar Star BS Circini*. p. 189  
 Mikulášek Z. Z., Krčička J., Jan'ik J., Henry G. W., Zejda M., Shultz M., Paunzen E., Jagelka M., 2017, in Balega Y. Y., Kudryavtsev D. O., Romanyuk I. I., Yakunin I. A., eds, *Astronomical Society of the Pacific Conference Series Vol. 510, Stars: From Collapse to Collapse*. p. 220 ([arXiv:1702.02195](https://arxiv.org/abs/1702.02195))  
 Netopil M., Paunzen E., Maitzen H. M., North P., Hubrig S., 2008, *A&A*, **491**, 545  
 Netopil M., Paunzen E., Hümmerich S., Bernhard K., 2017, *MNRAS*, **468**, 2745  
 Niemczura E., Hümmerich S., Castelli F., Paunzen E., Bernhard

- K., Hamsch F.-J., Helminiak K., 2017, *Scientific Reports*, **7**, 5906
- North P., 1984, *A&AS*, **55**, 259
- Ochsenbein F., Bauer P., Marcout J., 2000, *A&AS*, **143**, 23
- Oelkers R. J., et al., 2018, *AJ*, **155**, 39
- Oksala M. E., Wade G. A., Townsend R. H. D., Owocki S. P., Kochukhov O., Neiner C., Alecian E., Grunhut J., 2012, *MNRAS*, **419**, 959
- Paunzen E., 2004, in Zverko J., Ziznovsky J., Adelman S. J., Weiss W. W., eds, IAU Symposium Vol. 224, The A-Star Puzzle. pp 443–450, doi:10.1017/S1743921304004867
- Paunzen E., 2015, *A&A*, **580**, A23
- Paunzen E., Maitzen H. M., 1998, *A&AS*, **133**, 1
- Paunzen E., Vanmunster T., 2016, *Astronomische Nachrichten*, **337**, 239
- Paunzen E., Schnell A., Maitzen H. M., 2005, *A&A*, **444**, 941
- Paunzen E., Schnell A., Maitzen H. M., 2006, *A&A*, **458**, 293
- Pepper J., et al., 2007, *PASP*, **119**, 923
- Pepper J., Kuhn R. B., Siverd R., James D., Stassun K., 2012, *PASP*, **124**, 230
- Pigulski A., 2014, in Guzik J. A., Chaplin W. J., Handler G., Pigulski A., eds, IAU Symposium Vol. 301, Precision Asteroseismology. pp 31–38 (arXiv:1311.3954), doi:10.1017/S1743921313014038
- Pojmanski G., 2002, *Acta Astron.*, **52**, 397
- Preston G. W., 1974, *ARA&A*, **12**, 257
- Pyper D. M., Ryabchikova T., Malanushenko V., Kuschnig R., Plachinda S., Savanov I., 1998, *A&A*, **339**, 822
- Renson P., Manfroid J., 2009, *A&A*, **498**, 961
- Richer J., Michaud G., Turcotte S., 2000, *ApJ*, **529**, 338
- Romanyuk I. I., Semenko E. A., Yakunin I. A., Kudryavtsev D. O., 2013, *Astrophysical Bulletin*, **68**, 300
- Rufener F., 1981, *A&AS*, **45**, 207
- Samus N. N., Kazarovets E. V., Durlevich O. V., Kireeva N. N., Pastukhova E. N., 2017, *Astronomy Reports*, **61**, 80
- Shappee B. J., et al., 2014, *ApJ*, **788**, 48
- Shultz M. E., et al., 2019, *MNRAS*, **490**, 274
- Shulyak D., Krtićka J., Mikulášek Z., Kochukhov O., Lüftinger T., 2010, *A&A*, **524**, A66
- Sikora J., et al., 2019, *MNRAS*, **487**, 4695
- Smith D. P., Ryabchikova T., Malanushenko V., 1997, in American Astronomical Society Meeting Abstracts #190. p. 26.10
- Snellen I. A. G., et al., 2012, in Ground-based and Airborne Telescopes IV. p. 84440I (arXiv:1208.4116), doi:10.1117/12.925178
- Stibbs D. W. N., 1950, *MNRAS*, **110**, 395
- Talens G. J. J., Spronck J. F. P., Lesage A. L., Otten G. P. P. L., Stuik R., Pollacco D., Snellen I. A. G., 2017, *A&A*, **601**, A11
- Tetzlaff N., Neuhäuser R., Hohle M. M., 2011, *MNRAS*, **410**, 190
- Townsend R. H. D., Oksala M. E., Cohen D. H., Owocki S. P., ud-Doula A., 2010, *ApJ*, **714**, L318
- Vagnozzi S., 2019, *Atoms*, **7**
- Vassiliadis E., Wood P. R., 1993, *ApJ*, **413**, 641
- Wade G. A., et al., 2005, *A&A*, **442**, L31
- Wade G. A., Grunhut J. H., Marcolino W. L. F., Martins F., Howarth I. D., Nazé Y., Walborn N. R., Walborn 2011a, in Neiner C., Wade G., Meynet G., Peters G., eds, IAU Symposium Vol. 272, Active OB Stars: Structure, Evolution, Mass Loss, and Critical Limits. pp 220–221 (arXiv:1009.3564), doi:10.1017/S174392131101043X
- Wade G. A., et al., 2011b, *MNRAS*, **416**, 3160
- Watson C. L., 2006, Society for Astronomical Sciences Annual Symposium, **25**, 47
- Wenger M., et al., 2000, *A&AS*, **143**, 9
- Wraight K. T., White G. J., Bewsher D., Norton A. J., 2011, *MNRAS*, **416**, 2477
- Wraight K. T., Fossati L., Netopil M., Paunzen E., Rode-Paunzen M., Bewsher D., Norton A. J., White G. J., 2012, *MNRAS*, **420**, 757
- Zhao G., Zhao Y.-H., Chu Y.-Q., Jing Y.-P., Deng L.-C., 2012, *Research in Astronomy and Astrophysics*, **12**, 723
- van Leeuwen F., 2007, *A&A*, **474**, 653

## APPENDIX A: ESSENTIAL DATA FOR OUR SAMPLE STARS



**Table A1.** Essential data for the mostly new ACV variables analyzed with ASAS-3 and KELT data, sorted by data source and increasing right ascension. The columns denote: (1) Photometric survey source (A=ASAS-3; M=MASCARA; K=KELT). (2) HD number or other conventional identification. (3) Identification number from RM09. (4) Right ascension (J2000; GAIA DR2). (5) Declination (J2000; GAIA DR2). (6) Spectral type from RM09. (7) *V* magnitude range. (8) Period, derived in the present investigation. (9) Epoch (HJD-2450000). (10) Semi-amplitude of the fundamental variation ( $A_1$ ). (11) Semi-amplitude of the first harmonic variation ( $A_2$ ). (12) Phase of the fundamental variation ( $\phi_1$ ). (13) Phase of the first harmonic variation ( $\phi_2$ ). (14) *G* mag (GAIA DR2). (15) (*BP* - *RP*) index (GAIA DR2). Where available, classifications and periods from the VSX are provided in footnotes. The HD numbers of the four eclipsing binary systems in our sample are highlighted in bold font.

(1) Src	(2) Star	(3) #RM09	(4) $\alpha$ (J2000)	(5) $\delta$ (J2000)	(6) SpT [lit]	(7) <i>V</i> range [mag]	(8) Period [d]	(9) Epoch	(10) $A_1$ [mag]	(11) $A_2$ [mag]	(12) $\phi_1$ [rad]	(13) $\phi_2$ [rad]	(14) <i>G</i> [mag]	(15) ( <i>BP</i> - <i>RP</i> ) [mag]
A	TYC 4701-644-1	3920	02 32 01.69	-03 49 26.9	A0 Sr Eu	10.13-10.15	7.296(4)	3736.63(7)	0.009	0.002	0.496	0.661	10.139	0.273
A	HD 16504	4100	02 35 21.70	-68 09 40.0	B8 Si	9.02-9.03	3.3057(7)	4867.62(3)	0.005	0.002	0.287	0.838	9.021	-0.023
A	HD 25258	6438	04 00 38.96	-04 05 49.6	A2 Sr Eu	10.31-10.33	2.4490(4)	3806.47(2)	0.009	0.001	0.477	0.922	10.304	0.300
A	HD 28365 <sup>a</sup>	7280	04 27 56.40	-13 27 52.3	B9 Si	8.43-8.45	1.80606(9)	4685.91(2)	0.005	0.001	0.245	0.441	8.412	-0.107
A	HD 29925	7690	04 43 00.38	+01 06 28.4	B9 Si	8.32-8.34	0.665558(8)	2558.775(7)	0.007	0.002	0.222	0.624	8.294	-0.107
A	TYC 8510-712-1	8060	04 53 29.13	-53 39 26.4	A0 Si	10.54-10.55	10.263(8)	3652.8(1)	0.005	0.001	0.816	0.044	10.534	-0.092
A	HD 273763	8460	05 05 29.78	-47 53 24.0	A0 Sr	10.96-10.98	0.77418(2)	3430.557(8)	0.008	0.000	0.507	0.814	10.970	0.147
A	HD 36955	9740	05 35 04.54	-01 24 06.6	A2 Cr Eu	9.44-9.45	2.2848(2)	4590.46(2)	0.006	0.002	0.655	0.059	9.416	0.201
A	HD 40146 <sup>b</sup>	10710	05 56 58.90	-03 45 20.4	A0 Si	9.35-9.37	1.78216(8)	3759.68(2)	0.009	0.001	0.168	0.098	9.306	0.250
A	HD 42335 <sup>c</sup>	11290	06 10 05.33	-00 18 08.6	A0 Si	8.40-8.43	5.076(1)	3440.60(5)	0.013	0.004	0.876	0.451	8.358	0.139
A	HD 42510 <sup>d</sup>	11322	06 11 13.84	+03 51 46.5	A0 Si	9.01-9.10	1.90142(9)	3056.70(2)	0.012	0.035	0.555	0.551	9.052	0.149
A	HD 258686 <sup>e</sup>	12290	06 30 47.06	+10 03 46.4	B8 Si	9.12-9.13	1.47938(7)	2526.89(1)	0.006	0.002	0.749	0.552	9.398	-0.078
A	HD 46305	12400	06 32 06.36	-12 26 36.2	A0 Si	10.12-10.13	16.19(1)	2578.8(2)	0.007	0.001	0.526	0.292	10.082	-0.009
A	HD 46771	12540	06 34 34.15	-17 21 52.1	B9 Si	8.75-8.76	0.548205(6)	3734.691(5)	0.004	0.002	0.242	0.547	8.736	-0.011
A	HD 295354	12970	06 43 32.24	-03 24 09.6	A3-A9 Sr Eu	9.44-9.47	1.30194(3)	3015.71(1)	0.008	0.003	0.309	0.121	9.405	0.427
A	HD 49223	13280	06 47 47.77	+07 19 34.1	A0 Sr Eu	9.02-9.04	0.561189(7)	4531.584(6)	0.010	0.001	0.772	0.892	8.982	0.015
A	HD 49310	13320	06 48 10.73	+10 11 22.2	A0 Si	9.12-9.14	1.91912(9)	4762.85(2)	0.008	0.003	0.866	0.329	9.101	-0.094
A	HD 50090	13630	06 51 13.16	-11 25 47.5	A0 Si	9.32-9.34	0.86490(1)	3055.690(9)	0.005	0.002	0.837	0.649	9.977	-0.032
A	HD 50620	13880	06 51 38.38	-47 19 40.3	A3 Sr Eu Cr	9.74-9.75	12.73(1)	2171.8(1)	0.005	0.002	0.331	0.585	9.738	0.196
A	HD 50773	13950	06 54 37.04	-00 27 09.5	A2 Sr Cr Eu	9.37-9.39	1.04551(2)	3411.62(1)	0.009	0.002	0.663	0.594	9.362	0.168
A	HD 52156	14320	07 00 01.75	-02 06 07.3	A0 Si	9.30-9.32	1.65880(8)	3823.55(2)	0.009	0.002	0.782	0.602	9.275	-0.041
A	HD 55067 <sup>f</sup>	15016	07 10 51.44	-14 28 08.7	A4 Sr	9.22-9.28	1.09012(2)	5154.85(1)	0.030	0.002	0.025	0.563	9.257	0.441
A	HD 55094	15020	07 11 05.50	-11 32 34.7	B8 Si	10.26-10.30	4.1833(9)	3490.49(4)	0.018	0.005	0.294	0.053	10.344	0.146
A	TYC 6532-2200-1	15090	07 12 02.29	-27 43 04.9	B5 He	9.25-9.27	2.6412(5)	2877.91(3)	0.004	0.002	0.156	0.409	9.220	-0.251
A	HD 56882	15520	07 16 41.14	-46 21 17.4	F0 Sr Cr Eu	8.37-8.38	1.65475(7)	3089.62(2)	0.004	0.001	0.551	0.756	8.352	0.249
A	TYC 6545-2278-1	15830	07 22 55.93	-27 47 30.8	Si	10.10-10.15	0.695415(9)	2566.818(7)	0.021	0.001	0.710	0.738	10.301	-0.138
A	TYC 7104-2089-1	15860	07 23 21.48	-31 50 06.8	A Si	10.68-10.70	0.81842(2)	4487.617(8)	0.006	0.003	0.558	0.184	10.685	0.160
A	HD 57981	15800	07 23 24.47	-06 38 10.2	A0 Si	8.86-8.89	0.639702(8)	3636.883(6)	0.007	0.005	0.376	0.236	8.848	-0.069
A	HD 58097	15820	07 24 17.59	+05 47 30.8	A0 Si	9.41-9.43	0.567468(7)	4876.694(6)	0.007	0.002	0.902	0.352	9.425	-0.079
A	HD 58675	16030	07 25 14.91	-33 33 10.0	B9 Si	9.62-9.63	1.34887(3)	3278.84(1)	0.005	0.001	0.953	0.121	9.590	-0.063
A	HD 62562	17190	07 42 32.02	-45 02 00.0	A0 Sr Eu Cr	8.90-9.92	1.43748(6)	3731.81(1)	0.005	0.002	0.632	0.695	8.896	0.214
A	TYC 8143-3244-1 <sup>g</sup>	17740	07 52 48.67	-49 37 31.9	Si	9.14-9.20	2.1587(2)	1925.67(2)	0.025	0.008	0.770	0.323	9.111	-0.034
A	HD 68419	18920	08 10 00.54	-48 20 05.4	A2 Sr Cr Eu	8.18-8.19	1.50518(7)	4599.57(2)	0.005	0.001	0.867	0.092	8.174	0.079
A	HD 68998	19120	08 14 21.67	-16 11 08.7	A5 Eu Cr Sr	8.67-8.68	2.3768(3)	4539.59(2)	0.004	0.001	0.748	0.285	8.620	0.309
A	HD 71006	19610	08 20 28.08	-68 09 38.6	A0 Si	9.29-9.30	0.74340(1)	1884.758(7)	0.006	0.002	0.487	0.068	9.263	-0.107
A	TYC 8149-1763-1	19560	08 22 31.73	-45 18 12.8	Si	9.96-9.98	3.1844(7)	2961.78(3)	0.007	0.004	0.493	0.118	9.912	-0.050
A	HD 73455	20390	08 38 03.18	-16 02 15.3	A0 Sr Cr	10.26-10.29	5.977(1)	3127.58(6)	0.006	0.005	0.432	0.218	10.265	0.163
A	TYC 7144-2934-1	20500	08 38 24.32	-35 31 24.5	Si	9.75-9.76	2.04627(9)	1948.68(2)	0.005	0.001	0.496	0.028	9.709	0.107
A	HD 74611	20850	08 44 32.73	-13 11 36.9	B9 Si	9.53-9.54	7.551(4)	4468.75(8)	0.007	0.001	0.927	0.171	9.620	-0.172
A	HD 77546	21940	09 02 18.27	-28 35 48.4	A0 Si	9.42-9.45	3.9725(8)	3055.61(4)	0.007	0.004	0.661	0.334	9.436	0.024
A	HD 81141	23030	09 20 30.18	-66 29 20.9	B9 Si	8.02-8.04	1.27486(2)	3474.60(1)	0.007	0.001	0.244	0.150	7.974	0.077
A	HD 82038	23330	09 27 05.79	-59 22 10.2	A2 Sr Eu Cr	9.62-9.64	4.1808(9)	3184.50(4)	0.005	0.003	0.889	0.409	9.573	0.365
A	HD 83957	23960	09 39 51.91	-56 31 07.5	A0 Si	9.65-9.67	3.8513(8)	2947.84(4)	0.005	0.004	0.476	0.861	9.644	0.045
A	HD 86978	24860	10 00 44.94	-49 53 54.9	A0 Si	9.62-9.64	0.76767(1)	1954.678(8)	0.005	0.001	0.577	0.145	9.558	0.197
A	HD 87653 <sup>h</sup>	25130	10 04 45.97	-54 57 03.0	B9 Si	8.05-8.07	3.3065(7)	2676.56(3)	0.009	0.002	0.175	0.913	7.989	0.037
A	HD 88208	25260	10 08 29.43	-57 43 19.9	A0 Si	8.84-8.85	1.17626(3)	3495.57(1)	0.005	0.001	0.094	0.093	8.816	0.097
A	HD 88242	25280	10 09 05.39	-52 07 16.7	A0 Si Cr	9.41-9.43	0.581006(7)	4473.795(6)	0.007	0.001	0.686	0.035	9.386	0.037
A	HD 88701	25390	10 13 00.23	-37 30 12.5	B9 Cr Eu	9.27-9.33	25.77(2)	4756.9(3)	0.015	0.016	1.82	0.573	9.287	0.069
A	HD 89680 <sup>i</sup>	25750	10 19 53.49	-47 05 56.4	A0 Cr	8.42-8.43	2.1226(1)	1954.70(2)	0.007	0.001	0.863	0.936	8.409	0.110
A	HD 91337	26280	10 32 09.85	-29 16 39.2	A0 Cr Eu Sr	9.44-9.46	1.48162(6)	3775.81(1)	0.005	0.004	0.304	0.915	9.427	0.063
A	TYC 6074-361-1	26320	10 33 19.50	-21 05 11.5	Sr Cr Eu	9.73-9.75	5.656(1)	2027.55(6)	0.010	0.001	0.257	0.297	9.739	0.327
A	HD 91590	26350	10 33 32.41	-46 58 33.2	B9 Si	7.04-7.05	3.3169(7)	3410.80(3)	0.005	0.001	0.547	0.064	7.064	-0.103
A	HD 95198 <sup>j</sup>	27420	10 59 04.25	-34 52 34.0	B9 Si	7.82-7.84	0.97441(2)	3183.54(1)	0.011	0.001	0.585	0.562	7.829	-0.019
A	HD 95569	27530	11 00 35.89	-65 45 24.6	B9 Si	8.57-8.59	6.812(3)	3731.83(7)	0.005	0.001	0.925	0.841	8.514	0.256
A	HD 95508	27520	11 00 44.91	-50 25 46.7	A0 Cr	9.52-9.54	9.385(7)	1918.71(9)	0.006	0.001	0.315	0.852	9.500	0.078
A	HD 98956	28520	11 22 29.17	-62 27 19.6	B9 Si	8.63-8.66	46.62(6)	3052.7(5)	0.012	0.002	0.264	0.692	9.308	0.341
A	HD 100357 <sup>k</sup>	28840	11 32 06.06	-67 02 18.0	A0 Eu Cr Sr	8.99-9.02	1.62794(7)	2062.56(2)	0.007	0.012	0.982	0.766	8.970	0.125
A	HD 101089	29130	11 36 59.84	-74 02 16.6	B9 Si	9.25-9.26	0.540369(6)	3728.838(5)	0.005	0.001	0.199	0.717	9.128	0.534
A	HD 101600 <sup>l</sup>	29270	11 41 01.34	-60 36 48.2	A0 Si	8.55-8.58	4.4259(9)	4296.55(4)	0.011	0.003	0.009	0.208	8.525	0.067
A	HD 103300 <sup>m</sup>	29780	11 53 38.19	-49 19 13.9	A0 Sr Cr Eu	8.32-8.34	1.48098(7)	2676.78(1)	0.008	0.006	0.363	0.839	8.293	0.080
A	HD 110293 <sup>n</sup>	32050	12 41 45.29	-62 41 22.5	B9 Si	9.57-9.60	10.624(9)	3160.7(1)	0.012	0.006	0.399	0.634	9.478	0.362
A	HD 110446	32100	12 42 40.42	-56 52 25.2	B9 Cr Eu Si	9.40-9.42	4.2992(9)	3067.79(4)	0.005	0.004	0.152	0.641	9.394	0.323
A	HD 111672	32390	12 51 35.67	-52 35 31.8	B9 Si	9.84-9.86	1.00358(2)	4305.56(1)	0.010	0.003	0.625	0.085	9.810	-0.043
A	HD 112555	32740	12 58 23.36	-58 19 47.5	B8 Si	9.23-9.28	6.664(2)	3406.79(7)	0.020	0.005	0.588	0.280	9.162	0.225
A	HD 116419 <sup>o</sup>	33570	13 25 04.30	-63 10 33.0	B9 Si	8.57-8.58	4.638(1)	4507.78(5)	0.006	0.000	0.863	0.010	8.469	0.165

<sup>a</sup>NSV 16014 (ACV); <sup>b</sup>ASAS 3055659-0345.3 (MISC;  $P_{\text{VSX}} = 1.781649$  d); <sup>c</sup>HIP 29253 (VAR;  $P_{\text{VSX}} = 5.0782$  d); <sup>d</sup>ASAS J061114+0351.8 (EC)ESD;  $P_{\text{VSX}} = 1.9014$  d)  
<sup>e</sup>NSV 16881 (VAR); <sup>f</sup>ASAS J071051-1428.1 (DCEP-FO)ESD;  $P_{\text{VSX}} = 1.09015$  d); <sup>g</sup>ASAS J07

Table A1. continued.

(1) Src	(2) Star	(3) #RM09	(4) $\alpha$ (J2000)	(5) $\delta$ (J2000)	(6) SpT [lit]	(7) V range [mag]	(8) Period [d]	(9) Epoch	(10) $A_1$ [mag]	(11) $A_2$ [mag]	(12) $\phi_1$ [rad]	(13) $\phi_2$ [rad]	(14) $G$ [mag]	(15) $(BP - RP)$ [mag]
A	HD 116423	33580	13 25 26.47	-68 10 39.2	A0 Eu Sr Si	8.53-8.55	17.34(1)	5057.5(2)	0.008	0.002	0.021	0.174	8.425	0.269
A	HD 120059 <sup>P</sup>	34630	13 48 43.12	-58 47 16.3	B8 Si	8.83-8.85	4.1042(9)	2658.82(4)	0.011	0.001	0.936	0.054	8.790	0.098
A	HD 122264 <sup>Q</sup>	35060	14 02 24.91	-55 22 56.3	B9 Si	9.58-9.60	4.0490(8)	3815.70(4)	0.005	0.003	0.276	0.970	9.508	0.173
A	HD 123206	35320	14 08 15.62	-61 03 32.7	B9 Si	9.84-9.86	2.4328(4)	4879.84(2)	0.008	0.002	0.014	0.859	9.786	0.348
A	HD 123960 <sup>R</sup>	35460	14 12 47.73	-61 18 18.4	B9 Si	9.71-9.73	0.80499(1)	1964.715(8)	0.007	0.001	0.044	0.556	9.683	0.153
A	HD 129189 <sup>S</sup>	36840	14 45 32.98	-72 05 14.9	B9 Cr Eu	8.59-8.62	1.35563(4)	4109.87(1)	0.012	0.003	0.077	0.311	8.536	0.104
A	HD 133061	37780	15 04 23.30	-51 30 17.4	B9 Si	9.08-9.09	0.73512(1)	3901.669(7)	0.005	0.002	0.322	0.585	9.041	0.058
A	HD 134305 <sup>T</sup>	38130	16 04 44.86	+12 29 20.0	A0 Sr Cr Eu	7.25-7.27	1.03218(2)	2819.58(1)	0.006	0.001	0.184	0.235	7.207	0.275
A	HD 134121	38080	15 10 09.32	-52 10 03.3	B9 Si	10.00-10.02	1.27933(3)	2783.89(1)	0.005	0.001	0.652	0.737	9.974	0.167
A	HD 135459	38470	15 17 22.32	-53 43 39.0	A2 Eu Cr	9.94-9.97	0.92542(2)	2055.619(9)	0.011	0.005	0.297	0.349	9.950	0.526
A	HD 135714	38540	15 19 00.95	-56 34 41.2	A0 Si	10.14-10.16	4.0112(8)	3127.70(4)	0.007	0.001	0.008	0.116	10.085	0.102
A	HD 137436	39080	15 28 25.02	-53 25 12.1	B8 Si	8.80-8.83	2.2985(2)	4862.87(2)	0.009	0.004	0.970	0.558	8.826	0.368
A	HD 146971	41510	16 19 29.59	-09 37 30.1	A0 Sr Cr Eu	8.64-8.66	3.0512(6)	3128.76(3)	0.007	0.002	0.384	0.854	8.568	0.004
A	HD 147039	41540	16 22 18.20	-55 07 17.9	B8 Si	9.98-10.00	3.6142(7)	3657.51(4)	0.009	0.004	0.931	0.679	9.886	0.102
A	HD 147174	41590	16 25 11.94	-68 07 35.8	A0 Si Cr Sr	8.85-8.86	21.99(1)	3588.6(2)	0.004	0.001	0.651	0.220	9.248	0.080
A	HD 149046	42120	16 32 26.97	-07 11 04.4	A0 Sr Cr Eu	9.57-9.59	2.2103(2)	1949.88(2)	0.011	0.003	0.407	0.550	9.504	0.409
A	HD 149136	42170	16 34 42.53	-43 28 04.4	A0 Si	10.07-10.09	1.53894(8)	4298.75(2)	0.008	0.001	0.439	0.163	9.988	0.330
A	HD 150347 <sup>U</sup>	42510	16 41 35.48	-28 35 10.9	B9 Si	9.00-9.02	1.27630(3)	2031.73(1)	0.009	0.003	0.896	0.984	8.938	0.204
A	HD 150957	42670	16 46 31.78	-45 45 55.5	B8 Si	9.27-9.32	4.823(1)	4705.65(5)	0.020	0.002	0.029	0.561	9.251	0.113
A	HD 153149	43317	16 58 20.86	-17 28 05.1	A5 Sr Eu Cr	9.45-9.47	0.673791(9)	3189.591(7)	0.008	0.002	0.034	0.997	9.350	0.460
A	HD 154187	43585	17 04 27.12	-14 03 36.5	A0 Si	9.26-9.29	8.096(5)	3467.83(8)	0.011	0.003	0.409	0.072	9.086	0.813
A	HD 154253	43610	17 08 09.00	-60 45 03.2	A0 Sr Cr Eu	9.05-9.06	3.0919(6)	3487.79(3)	0.006	0.002	0.670	0.846	8.990	0.281
A	HD 154458	43660	17 09 12.81	-59 48 49.3	B9 Si	8.27-8.30	4.4573(9)	3564.62(4)	0.009	0.002	0.096	0.043	8.253	-0.045
A	TYC 8336-2364-1	43760	17 11 15.23	-50 09 56.1	Si	9.94-9.95	2.0840(1)	3571.59(2)	0.006	0.002	0.840	0.309	9.869	0.252
A	HD 156366	44050	17 18 15.66	-28 07 21.4	A2 Sr Eu	9.68-9.70	3.8057(8)	4227.79(4)	0.008	0.003	0.676	0.049	9.548	0.606
A	HD 158234 <sup>V</sup>	44510	17 29 38.16	-35 46 26.3	A0 Si	9.50-9.58	2.6825(5)	1953.84(3)	0.042	0.004	0.421	0.706	9.446	0.214
A	HD 161445	45496	17 45 23.11	+05 33 45.6	A0 Si Eu Sr	10.09-10.11	2.1568(1)	2711.86(2)	0.006	0.002	0.335	0.128	10.057	0.198
A	HD 162306 <sup>W</sup>	45790	17 51 55.23	-35 04 57.6	B9 Si	8.67-8.70	1.70249(8)	3582.74(2)	0.014	0.002	0.309	0.321	8.859	0.019
A	HD 162639	45930	17 54 41.33	-50 26 45.9	A5 Sr Eu Cr	9.86-9.90	39.82(4)	3093.9(4)	0.013	0.001	0.018	0.634	9.821	0.537
A	HD 163583	46280	18 00 05.31	-55 37 58.4	A3 Sr Cr Eu	10.49-10.51	1.38313(6)	3584.81(1)	0.006	0.001	0.919	0.137	10.434	0.315
A	HD 164068	46388	18 00 24.15	-22 57 52.2	A0 Si	9.70-9.73	2.4133(3)	3573.64(2)	0.013	0.003	0.984	0.867	9.783	0.271
A	HD 167024	47010	18 15 07.57	-38 53 39.7	A2 Sr Eu	9.19-9.22	3.0934(7)	3178.66(3)	0.006	0.006	0.088	0.708	9.142	0.239
A	HD 168071	47115	18 17 58.30	+03 28 47.7	A0 Sr Eu Cr	8.61-8.62	2.3122(3)	2529.52(2)	0.005	0.001	0.795	0.733	8.509	0.505
A	HD 168108	47120	18 20 33.49	-47 58 39.0	B8 Si	8.67-8.69	1.42776(5)	2441.69(1)	0.006	0.002	0.710	0.277	8.621	-0.008
A	HD 169021 <sup>X</sup>	47410	18 24 03.93	-34 20 02.7	B9 Si	7.00-7.05	3.0955(7)	4578.86(3)	0.019	0.008	0.601	0.273	6.954	-0.009
A	TYC 7415-2499-1	48010	18 36 06.66	-35 08 34.5	Si	9.76-9.79	149.4(1)	2904.5(9)	0.015	0.002	0.260	0.991	9.759	0.038
A	HD 171914	48170	18 37 12.19	+02 58 34.4	A0 Si Sr Eu	7.87-7.89	1.65793(7)	2882.61(2)	0.007	0.001	0.053	0.609	7.838	0.133
A	HD 172251	48263	18 39 17.24	-03 09 04.2	B9 Si	9.21-9.23	4.5498(9)	2862.73(5)	0.009	0.001	0.587	0.204	9.060	0.649
A	HD 172626	48360	18 42 51.08	-37 04 37.4	A2 Sr Cr Eu	9.69-9.70	12.32(1)	5024.7(1)	0.005	0.001	0.905	0.373	9.630	0.305
A	HD 177016	49374	19 03 40.57	-20 34 36.9	F0 Eu Sr Cr	9.29-9.31	1.64041(7)	1994.85(2)	0.006	0.002	0.804	0.500	9.213	0.498
A	HD 230952	49970	19 14 13.57	+14 23 30.4	A0 Si	9.47-9.49	1.42820(5)	3133.84(1)	0.010	0.001	0.475	0.614	9.399	0.421
A	HD 181028	50184	19 19 06.74	-06 59 22.9	A2 Sr Eu Cr	10.11-10.12	7.457(3)	2134.59(7)	0.006	0.001	0.582	0.039	10.006	0.675
A	HD 184020 <sup>Y</sup>	50800	19 34 42.78	-49 41 05.4	A0 Sr Cr Eu	8.15-8.17	2.5515(5)	3552.85(3)	0.007	0.003	0.292	0.842	8.126	0.017
A	HD 185280	51180	19 40 11.30	-40 52 32.0	A2 Cr Eu	8.42-8.44	1.35464(3)	3190.75(1)	0.006	0.001	0.260	0.132	9.428	0.150
A	HD 193382	54000	20 21 56.75	-47 43 24.6	A0 Si Cr Eu	9.86-9.89	8.374(6)	1996.86(4)	0.009	0.003	0.450	0.683	9.850	0.600
A	HD 209051	58130	22 00 39.98	-06 25 57.0	A0 Si Cr Eu	9.76-9.78	0.69640(1)	2216.569(7)	0.006	0.002	0.714	0.100	8.738	-0.048
A	HD 222638	61030	23 02 33.97	-57 28 40.9	A0 Sr Cr Eu	8.65-8.66	1.17352(3)	2145.71(1)	0.004	0.002	0.324	0.864	8.650	0.057
K	HD 7410	1860	01 14 40.41	+33 00 04.8	A5 Sr Cr Eu	9.07-9.09	37.08(2)	4054.7(3)	0.010	0.002	0.435	0.047	9.066	0.325
K	HD 9393	2270	01 33 15.52	+43 53 45.1	B9 Si Cr Sr	8.60-8.61	2.4998(3)	4035.52(2)	0.003	0.002	0.528	0.075	8.600	-0.082
K	HD 9492	2300	01 34 08.06	+44 05 38.3	A0 Si Cr	8.46-8.48	10.898(6)	4421.7(1)	0.006	0.002	0.918	0.288	8.432	0.096
K	TYC 2816-447-1	3063	01 58 12.70	+37 34 40.5	F2 Sr	10.95-10.96	0.73356(2)	4057.684(7)	0.002	0.001	0.296	0.459	10.853	0.538
K	HD 13404	3470	02 11 54.03	+36 57 58.3	A2 Sr Eu	8.74-8.75	4.358(2)	4037.71(4)	0.002	0.000	0.212	0.686	8.733	0.371
K	HD 14522	3660	02 21 20.03	+28 04 15.8	A2 Sr Eu	8.80-8.81	26.36(1)	4059.3(2)	0.004	0.002	0.681	0.900	8.749	0.327
K	HD 16605	4140	02 40 58.94	+42 52 16.6	A1 Si Cr Sr	9.56-9.57	8.820(4)	4034.79(8)	0.003	0.003	0.169	0.940	9.618	0.072
K	TYC 2850-263-1	4480	02 53 02.19	+39 55 12.5	A Sr Cr Eu	9.79-9.80	12.440(8)	4052.5(1)	0.003	0.001	1.000	0.277	9.646	0.510
K	TYC 2854-1633-1	4520	02 57 10.63	+43 04 43.8	Sr Eu	9.73-9.74	13.448(8)	4387.7(1)	0.006	0.003	0.617	0.128	9.695	0.452
K	TYC 2394-739-1	8844	05 20 31.61	+32 36 14.1	B9 Si	11.00-11.01	4.464(2)	4061.80(4)	0.007	0.001	0.993	0.969	10.972	0.371
K	HD 243308	9006	05 24 58.17	+30 04 46.5	B9 Si	10.78-10.79	1.7209(2)	4385.92(1)	0.003	0.001	0.136	0.525	10.771	0.228
K	HD 243494	9080	05 26 12.31	+32 02 03.5	B9 Si	9.65-9.67	3.0124(2)	4417.84(2)	0.008	0.004	0.076	0.825	9.520	0.241
K	HD 243492	9082	05 26 16.49	+33 15 44.3	A0 Si Sr	10.63-10.65	2.9317(2)	4386.98(2)	0.007	0.000	0.366	0.036	10.602	0.350
K	<b>HD 244391</b>	9357	05 31 41.47	+31 37 25.0	B8 Si Sr	10.35-10.41	6.0783(4)	4422.27(2)	-	-	-	-	10.260	0.507
K	TYC 2412-1235-1	9655	05 36 02.39	+34 06 50.9	B9 Si	9.87-9.88	0.55386(1)	4040.938(5)	0.003	0.001	0.750	0.845	9.959	0.089
K	HD 245601	9953	05 38 08.91	+29 00 36.1	B9 Si Sr	9.84-9.85	1.57095(7)	4056.79(1)	0.003	0.000	0.358	0.008	9.170	1.901
K	HD 246820	10239	05 44 16.39	+27 57 18.7	A0 Si Sr	10.54-10.57	1.29620(3)	4117.67(1)	0.014	0.001	0.022	0.408	10.511	0.315
K	TYC 2413-822-1	10316	05 46 29.38	+34 13 34.6	B8 Si	10.18-10.19	1.41839(7)	4059.77(1)	0.003	0.001	0.457	0.337	10.156	0.156
K	<b>HD 247441<sup>Z</sup></b>	10334	05 47 04.35	+28 13 44.7	B9 Si Sr	9.05-9.16	4.26756(5)	4061.70(1)	-	-	-	-	9.050	0.119
K	GSC 2413-00426	10391	05 48 36.91	+33 52 56.1	A3 Sr	11.92-11.93	1.5810(2)	4037.81(1)	0.006	0.001	0.896	0.562	11.870	0.475
K	HD 38979	10476	05 50 53.58	+30 43 24.5	B7 Si	9.17-9.21	2.56099(4)	4746.89(2)	0.021	0.003	0.269	0.409	9.197	0.077
K	<b>HD 248784</b>	10593	05 54 04.81	+34 01 50.2	B8 Si Sr	9.59-9.71	0.81821(1)	4057.835(4)	-	-	-	-		

Table A1. continued.

(1) Src	(2) Star	(3) #RM09	(4) $\alpha$ (J2000)	(5) $\delta$ (J2000)	(6) SpT [lit]	(7) V range [mag]	(8) Period [d]	(9) Epoch	(10) $A_1$ [mag]	(11) $A_2$ [mag]	(12) $\phi_1$ [rad]	(13) $\phi_2$ [rad]	(14) $G$ [mag]	(15) $(BP - RP)$ [mag]
K	TYC 3161-135-1 <sup>aa</sup>	54600	20 32 12.87	+43 03 57.5	B9 Si	9.11-9.14	1.09626(3)	4273.88(1)	0.018	0.001	0.136	0.626	9.111	-0.025
K	HD 196542	54800	20 36 43.34	+39 06 14.8	A4 Sr Cr Eu	9.03-9.05	1.7929(1)	4265.85(1)	0.010	0.002	0.528	0.256	9.038	0.112
K	HD 197560	55080	20 43 17.78	+35 44 30.1	A0 Si	7.99-8.03	2.8812(2)	4270.81(2)	0.012	0.007	0.420	0.261	7.981	-0.052
K	HD 198195	55170	20 47 09.92	+42 24 35.4	B8 Si	7.43-7.45	1.49665(7)	4588.87(1)	0.008	0.001	0.673	0.454	7.417	-0.061
K	TYC 2696-483-1	55400	20 52 44.75	+34 13 00.8	Si	10.18-10.20	3.5031(2)	4380.61(3)	0.011	0.003	0.235	0.841	10.226	0.074
K	TYC 2713-1881-1	56156	21 07 40.45	+35 54 02.8	B8 Si	10.56-10.58	0.75430(2)	4268.851(7)	0.007	0.003	0.528	0.003	10.444	-0.089
K	HD 203786	56730	21 23 54.71	+21 55 50.8	B9 Si	8.00-8.01	5.398(2)	4277.80(5)	0.004	0.003	0.133	0.853	7.988	-0.091
K	HD 205087 <sup>ab</sup>	57120	21 32 27.01	+23 23 40.5	A0 Sr Si Cr	6.67-6.68	0.59774(1)	4275.933(5)	0.002	0.000	0.222	0.988	6.657	-0.065
K	HD 206898	57560	21 44 20.80	+35 15 18.3	A0 Si	8.57-8.60	1.6485(1)	4261.87(1)	0.009	0.006	0.553	0.138	8.565	0.047
K	HD 209059	58140	22 00 06.67	+26 47 01.8	B9 Si	7.72-7.73	3.3551(2)	4276.81(3)	0.002	0.001	0.029	0.371	7.714	-0.029

<sup>aa</sup>HIP 101323 (SPB;  $P_{\text{VSX}} = 1.09613$  d); <sup>ab</sup>NSV 13774 (no type and period given)

**Table A2.** Essential data for the known ACV variables whose rotational periods were investigated with MASCARA data, sorted by increasing right ascension. The columns denote: (1) HD number or other conventional identification. (2) Identification number from RM09. (3) Right ascension (J2000; GAIA DR2). (4) Declination (J2000; GAIA DR2). (5) Spectral type from RM09. (6)  $V$  magnitude range. (7) Literature period (VSX). (8) Period (this work). (9) Epoch (HJD-2450000). (10) Semi-amplitude of the fundamental variation ( $A_1$ ). (11) Semi-amplitude of the first harmonic variation ( $A_2$ ). (12) Phase of the fundamental variation ( $\phi_1$ ). (13) Phase of the first harmonic variation ( $\phi_2$ ). (14)  $G$  mag (GAIA DR2). (15) ( $BP - RP$ ) index (GAIA DR2).

(1) Star	(2) #RM09	(3) $\alpha$ (J2000)	(4) $\delta$ (J2000)	(5) SpT [lit]	(6) $V$ range [mag]	(7) $P_{VSX}$ [d]	(8) $P_{MASCARA}$ [d]	(9) Epoch	(10) $A_1$ [mag]	(11) $A_2$ [mag]	(12) $\phi_1$ [rad]	(13) $\phi_2$ [rad]	(14) $G$ [mag]	(15) $(BP - RP)$ [mag]
HD 3580	970	00 38 31.86	-20 17 47.6	B8 Si	6.71-6.73	1.4788	1.47561(4)	7219.71(1)	0.006	0.001	0.986	0.484	6.687	-0.157
HD 4778	1250	00 50 18.27	+45 00 08.2	A1 Cr Sr Eu	6.10-6.13	2.5481	2.5619(1)	7185.70(2)	0.006	0.008	0.899	0.974	6.110	0.028
HD 4796	1263	00 52 28.98	+79 50 25.6	A0 Sr Si	7.71-7.73	8	7.987(2)	7060.62(7)	0.009	0.000	0.765	0.323	7.695	0.152
HD 7676	1880	01 16 06.81	-34 08 55.8	A5 Sr Cr Eu	8.36-8.41	5.0976	5.088(2)	7252.84(5)	0.022	0.007	0.010	0.744	8.388	0.217
HD 7546	1870	01 16 24.50	+48 04 56.1	B8 Si	6.60-6.62	5.229	5.4060(9)	7057.38(5)	0.009	0.004	0.250	0.826	6.563	-0.002
HD 8441	2050	01 24 18.69	+43 08 31.6	A2 Sr	6.66-6.68	69.92	69.9(1)	7230.2(7)	0.009	0.004	0.228	0.942	6.651	0.079
HD 10221	2550	01 42 20.51	+68 02 34.9	A0 Si Sr Cr	5.54-5.58	3.1848	3.1528(2)	7216.49(3)	0.017	0.005	0.769	0.899	5.529	-0.064
HD 10783	2670	01 45 42.52	+08 33 33.2	A2 Si Cr Sr	6.53-6.56	4.1321	4.1335(3)	7057.30(4)	0.009	0.005	0.374	0.063	6.514	-0.009
HD 11415	2870	01 54 23.74	+63 40 12.4	B3 He wk.	3.34-3.35	<b>0.08946</b>	<b>14.53(1)</b>	7192.6(1)	0.006	0.002	0.528	0.503	3.261	0.070
HD 12288	3130	02 03 30.49	+69 34 56.4	A2 Cr Si	7.72-7.74	34.9	35.73(3)	7218.6(3)	0.007	0.002	0.772	0.633	7.706	0.177
HD 14392	3620	02 20 58.20	+40 09 05.4	B9 Si	5.55-5.57	4.189	4.2143(5)	7060.59(4)	0.006	0.002	0.298	0.078	5.522	-0.098
HD 14437	3640	02 21 02.67	+42 56 38.2	B9 Cr Eu Si	7.24-7.27	26.87	26.78(1)	7077.7(2)	0.013	0.002	0.427	0.530	7.221	0.005
HD 16545	4120	02 40 36.94	+19 04 28.4	A0 Si	7.33-7.37	1.61942	1.61905(5)	7068.33(1)	0.022	0.002	0.061	0.080	7.333	-0.107
HD 18296	4560	02 57 17.28	+31 56 03.3	A0 Si Sr	5.08-5.10	2.88422	2.8836(2)	7065.37(2)	0.007	0.006	0.585	0.386	5.074	-0.039
HD 18473	4610	03 00 53.79	+59 39 57.6	B9 Si	7.33-7.35	0.666832	0.66690(1)	7057.334(6)	0.009	0.001	0.480	0.039	7.306	0.026
HD 19712	4880	03 10 18.09	-01 41 41.0	A0 Cr Eu	7.31-7.33	2.1945	2.2045(1)	7064.37(2)	0.007	0.007	0.230	0.574	7.306	-0.039
HD 19832	4910	03 12 14.25	+27 15 25.1	B8 Si	5.76-5.81	0.727902	0.72795(1)	7059.386(7)	0.015	0.011	0.965	0.645	5.752	-0.133
HD 20629	5160	03 19 47.76	+19 04 34.6	A0 Si Sr Cr	7.36-7.45	2.4994	2.49934(6)	7059.38(2)	0.045	0.004	0.264	0.680	7.377	-0.043
HD 21590	5400	03 29 42.57	+16 45 44.4	B9 Si	7.03-7.05	2.7609	2.7586(2)	7057.27(2)	0.004	0.001	0.487	0.325	7.009	-0.018
HD 21699	5410	03 32 08.60	+48 01 24.6	B8 He wk. Si	7.45-7.47	2.4761	2.4928(2)	7059.37(2)	0.011	0.001	0.848	0.013	5.410	-0.109
HD 22136	5570	03 35 58.49	+47 05 27.8	B8 Si	6.86-6.88	0.9312	0.93111(3)	7077.412(9)	0.011	0.001	0.737	0.230	6.852	-0.009
HD 22470	5710	03 36 17.39	-17 28 01.6	B9 Si	5.21-5.27	1.93	1.92911(7)	7067.48(1)	0.021	0.013	0.013	0.669	5.145	-0.157
HD 22374	5660	03 36 58.03	+23 12 39.9	A1 Cr Sr Si	6.71-6.73	10.61	10.656(2)	7083.4(1)	0.008	0.003	0.174	0.111	6.687	0.172
HD 22920	5840	03 40 38.34	-05 12 38.6	B8 Si	5.51-5.55	3.9474	3.9489(3)	7060.57(3)	0.019	0.006	0.651	0.045	5.485	-0.173
HD 24155	6190	03 51 15.86	+13 02 46.0	B9 Si	6.27-6.33	2.53465	2.5348(1)	7080.55(2)	0.029	0.003	0.422	0.726	6.247	-0.050
HD 24769	6330	03 57 03.80	+23 10 32.2	B9 Si	6.03-6.06	1.48778	1.48759(4)	7066.50(1)	0.019	0.000	0.436	0.597	6.009	0.104
HD 25267	6440	03 59 55.48	-24 00 58.8	A0 Si	4.62-4.63	1.2094	1.20971(4)	7262.65(1)	0.007	0.001	0.095	0.652	4.561	-0.126
HD 25354	6460	04 03 10.85	+38 03 17.3	A2 Eu Cr	7.82-7.84	3.90072	3.9021(5)	7066.61(3)	0.014	0.001	0.758	0.111	7.825	0.044
HD 25823	6560	04 06 36.41	+27 35 59.5	B9 Sr Si	7.72-7.73	7.227424	7.238(2)	7080.45(7)	0.009	0.001	0.513	0.708	5.133	-0.159
HD 26792	6840	04 17 21.08	+57 10 41.9	B8 Sr	6.67-6.71	3.8031	3.8023(3)	7128.33(3)	0.019	0.008	0.995	0.225	6.683	0.068
HD 26961	6880	04 18 14.61	+50 17 43.8	A2 Si	4.57-4.62	1.5273643	1.52730(7)	7056.37(1)	0.006	0.023	0.421	0.463	4.511	0.112
HD 27309	7010	04 19 36.70	+21 46 24.7	A0 Si Cr	5.33-5.38	1.56896	1.56882(5)	7056.40(1)	0.025	0.007	0.758	0.178	5.319	-0.124
HD 27404	7030	04 20 37.78	+28 53 31.3	A0 Si	7.90-7.95	2.77929	2.7789(2)	7087.42(2)	0.024	0.003	0.366	0.851	7.833	0.413
HD 28843	7380	04 32 37.56	-03 12 34.4	B9 He wk. Si	5.70-5.80	1.374	1.37393(2)	7059.50(1)	0.047	0.003	0.558	0.378	5.740	-0.161
HD 29009	7420	04 33 54.73	-06 44 20.1	B9 Si	5.71-5.73	3.82	3.7993(4)	7057.40(3)	0.007	0.003	0.209	0.627	5.723	-0.164
HD 30466	7870	04 49 16.00	+29 34 16.9	A0 Si	7.24-7.27	1.4069	1.40687(4)	7059.49(1)	0.011	0.003	0.898	0.048	7.194	0.190
HD 32145	8190	05 01 06.03	+03 03 02.4	B7 Si	7.22-7.25	2.42082	2.4190(1)	7067.48(2)	0.009	0.004	0.151	0.454	7.199	-0.148
HD 32549	8280	05 04 34.14	+15 24 15.0	B9 Si Cr	4.65-4.68	4.6397	4.6393(4)	7060.31(4)	0.015	0.002	0.942	0.707	4.610	-0.045
HD 32633	8320	05 06 08.35	+33 55 07.3	B9 Si Cr	7.04-7.07	6.43	6.4303(8)	7059.85(6)	0.009	0.004	0.774	0.997	7.001	0.010
HD 32966	8420	05 06 22.15	-14 41 47.6	B9 Si	7.06-7.17	3.0929	3.0928(1)	7057.20(3)	0.052	0.006	0.868	0.213	7.097	-0.098
HD 32650	8350	05 12 22.43	+73 56 47.9	B9 Si	5.40-5.45	2.73475	2.7353(1)	7143.31(2)	0.021	0.002	0.202	0.650	5.392	-0.128
HD 34719	8850	05 20 18.29	+19 34 41.7	A0 Hg Si Cr	6.63-6.66	1.63988	1.64000(5)	7059.43(1)	0.012	0.007	0.193	0.752	6.625	-0.036
HD 36916	9700	05 34 53.96	-04 06 37.6	B8 He wk. Si	6.71-6.75	1.564	1.56520(5)	7066.32(1)	0.017	0.004	0.042	0.594	6.680	-0.165
HD 37808	10210	05 40 46.19	-10 24 31.1	B9 Si	6.44-6.46	1.099	1.09852(2)	7096.33(1)	0.009	0.002	0.888	0.969	6.419	-0.157
HD 38823	10440	05 48 25.50	-00 45 34.6	A5 Sr Eu Cr	7.31-7.33	8.635	8.677(2)	7087.98(8)	0.010	0.006	0.062	0.875	7.315	0.387
HD 39082	10500	05 50 23.86	+04 57 24.1	B9 Sr Cr Eu	7.39-7.41	0.764776	0.76477(2)	7059.487(7)	0.010	0.001	0.900	0.484	7.389	0.032
HD 39317	10560	05 52 22.30	+14 10 18.5	B9 Si Eu Cr	5.59-5.60	2.6569	2.6558(3)	7059.49(2)	0.005	0.001	0.974	0.216	5.561	-0.036
HD 39575	10600	05 52 23.85	-26 17 28.1	A0 Si Cr Eu	7.82-7.85	3.1009	3.1014(2)	7301.74(3)	0.015	0.004	0.461	0.901	7.811	0.001
HD 42616	11390	06 13 43.15	+41 41 50.2	A1 Sr Cr Eu	7.15-7.16	<b>17</b>	<b>5.739(1)</b>	7057.16(5)	0.008	0.000	0.137	0.511	7.113	0.186
HD 43819	11620	06 19 01.86	+17 19 30.9	B9 Si	6.26-6.28	15.0285	14.981(6)	7065.8(1)	0.007	0.004	0.092	0.483	6.236	-0.079
HD 45439	12040	06 25 42.46	-35 41 50.5	B9 Si	7.84-7.90	1.10064	1.10059(2)	7064.44(1)	0.028	0.003	0.979	0.320	7.839	-0.043
HD 45530	12070	06 28 13.96	+05 16 20.2	A0 Si	7.47-7.49	0.7919	0.79187(2)	7065.622(7)	0.011	0.000	0.024	0.029	7.607	-0.043
HD 46462	12430	06 31 45.20	-37 10 23.2	B9 Si	7.50-7.56	10.363	10.346(5)	7080.9(1)	0.022	0.015	0.388	0.989	7.519	-0.115
HD 47144	12660	06 35 24.18	-36 46 47.5	B9 Si	5.76-5.77	2.21004	2.2111(2)	7081.32(2)	0.007	0.002	0.014	0.442	5.905	-0.128
HD 47714	12810	06 39 32.66	-11 41 51.6	B8 Si	7.92-7.96	4.6953	4.6955(4)	7057.48(4)	0.017	0.004	0.725	0.209	7.949	-0.051
HD 49333	13340	06 47 01.48	-21 00 55.4	B7 He wk. Si	6.05-6.08	2.181	2.1805(1)	7066.71(2)	0.014	0.005	0.716	0.142	6.207	-0.221
HD 49484	13390	06 47 47.12	-22 10 10.3	B9 Si	8.32-8.35	7.039	7.033(1)	7068.55(7)	0.017	0.002	0.697	0.929	8.338	-0.134
HD 49713	13480	06 49 44.29	-01 20 23.7	B9 Cr Eu Si	7.29-7.34	2.13503	2.13512(8)	7060.56(2)	0.023	0.004	0.924	0.844	7.281	-0.077
HD 49976	13560	06 50 42.30	-08 02 27.6	A1 Sr Cr Eu	6.28-6.32	2.976	2.9768(2)	7067.30(2)	0.009	0.010	0.454	0.908	6.280	0.043
HD 50304	13774	06 51 41.36	-23 48 10.4	A0 Eu Cr	7.54-7.58	7.884	7.886(1)	7287.92(7)	0.022	0.002	0.589	0.352	7.544	0.058
HD 50461	13810	06 53 08.00	-07 45 56.1	B9 Si Cr	7.79-7.82	0.89403	0.89400(2)	7059.427(8)	0.011	0.005	0.377	0.695	7.778	-0.065
HD 50341	13780	06 54 13.60	+33 00 09.1	B9 Sr Cr Eu	8.16-8.20	2.50919	2.5094(1)	7060.58(2)	0.019	0.008	0.036	0.514	8.166	0.036
HD 51418	14180	06 59 20.14	+42 18 53.2	A0 Ho Dy	6.60-6.73	5.4379	5.4377(3)	7065.44(5)	0.069	0.011	0.413	0.048	6.664	0.099
HD 52993	14550	07 01 47.21	-35 32 52.5	B9 Si	6.54-6.61	1.29644	1.29645(3)	7057.37(1)	0.025	0.018	0.295	0.460	6.540	-0.182
HD 56273	15300	07 15 57.31	-12 32 35.2	B8 Si	7.88-7.92	1.78661	1.78678(6)	7064.46(1)	0.017	0.008	0.027	0.288	7.892	-0.060
HD 59256	16180	07 27 59.16	-29 09 21.2	B9 Si	5.54-5.55	0.943	0.94343(3)	7067.558(9)	0.006	0.000	0.411	0.647	5.508	



Table A2. continued.

(1)	(2)	(3)	(4)	(5)	(6)	(7)	(8)	(9)	(10)	(11)	(12)	(13)	(14)	(15)
Star	#RM09	$\alpha$ (J2000)	$\delta$ (J2000)	SpT	V range	PV SX	PMASCARA	Epoch	A <sub>1</sub>	A <sub>2</sub>	$\phi_1$	$\phi_2$	G	(BP - RP)
				[lit]	[mag]	[d]	[d]		[mag]	[mag]	[rad]	[rad]	[mag]	[mag]
HD 71866	19850	08 31 10.65	+40 13 29.7	A1 Eu Sr Si	6.70-6.72	6.80054	6.797(1)	7097.20(6)	0.004	0.005	0.478	0.301	6.703	0.089
HD 77314	21834	09 01 58.77	+02 40 16.5	A2 Sr Cr Eu	7.20-7.28	2.8646	2.86445(8)	7056.66(2)	0.030	0.016	0.216	0.704	7.267	0.104
HD 93226	26920	10 45 48.22	-10 42 48.8	A0 Si	7.43-7.48	1.72907	1.72913(6)	7057.77(1)	0.018	0.004	0.108	0.233	7.459	-0.033
HD 95442	27500	11 00 44.05	-25 43 02.4	A0 Sr Cr Eu	7.82-7.84	3.3386	3.3384(3)	7122.58(3)	0.010	0.005	0.220	0.639	7.823	0.084
HD 96707	27890	11 09 39.78	+67 12 36.9	A8 Sr	7.06-7.07	3.51556	3.5129(5)	7140.34(3)	0.006	0.002	0.189	0.424	6.023	0.302
HD 98457	28360	11 19 25.95	-30 19 22.9	A0 Si	7.90-7.98	11.534	11.533(2)	7085.4(1)	0.043	0.009	0.387	0.958	7.919	-0.058
HD 102454	29530	11 47 26.22	-31 15 17.0	B9 Si	7.30-7.32	2.07906	2.0792(1)	7071.51(2)	0.008	0.006	0.747	0.339	7.287	-0.029
HD 111133	32310	12 47 02.30	+05 57 01.3	A1 Sr Cr Eu	6.28-6.31	<b>2.2246</b>	<b>16.230(5)</b>	7060.0(1)	0.014	0.002	0.577	0.591	6.276	0.003
HD 118022	34020	13 34 07.95	+03 39 32.4	A2 Cr Eu Sr	4.90-4.92	3.722	3.7216(4)	7065.52(3)	0.008	0.002	0.212	0.838	4.854	0.058
HD 119213	34410	13 40 21.37	+57 12 27.6	A3 Sr Cr	6.27-6.28	2.449967	2.4478(2)	7132.73(2)	0.007	0.001	0.815	0.681	6.266	0.088
HD 124224	35560	14 12 15.81	+02 24 33.8	B9 Si	4.95-5.02	0.52071601	0.520700(3)	7064.698(5)	0.036	0.004	0.064	0.894	4.950	-0.103
HD 125248	35760	14 18 38.26	-18 42 57.5	A1 Eu Cr	5.83-5.86	9.2954	9.302(1)	7067.40(9)	0.006	0.008	0.985	0.216	5.844	0.009
HD 133029	37770	15 00 38.72	+47 16 38.8	B9 Si Cr Sr	6.34-6.36	2.8881	2.8885(2)	7095.68(2)	0.008	0.001	0.208	0.115	6.319	-0.106
HD 138764	39510	15 34 26.51	-09 11 00.3	B6 Si	5.12-5.17	1.25881	1.25869(3)	7070.74(1)	0.020	0.001	0.228	0.643	5.103	-0.108
HD 140160	39840	15 41 47.42	+12 50 51.2	A1 Sr	5.31-5.33	1.59584	1.59590(8)	7057.78(1)	0.010	0.004	0.167	0.057	5.292	0.045
HD 142884	40510	15 57 48.81	-23 31 38.3	B9 Si	6.76-6.78	0.803	0.80296(2)	7058.762(8)	0.006	0.004	0.829	0.922	6.719	0.068
HD 148112	41850	16 25 24.95	+14 01 59.8	A0 Cr Eu	4.56-4.58	2.951	3.0439(3)	7058.87(3)	0.011	0.004	0.813	0.577	4.497	0.037
HD 151199	42760	16 42 58.46	+55 41 24.4	A3 Sr	6.16-6.17	2.226	2.2267(2)	7058.66(2)	0.005	0.003	0.795	0.820	6.158	0.097
HD 150714	42640	16 43 39.68	-22 44 11.1	A0 Si	7.54-7.59	1.6288	1.62906(5)	7087.73(1)	0.018	0.013	0.930	0.109	7.523	0.245
HD 152107	43050	16 49 14.23	+45 59 00.1	A3 Sr Cr Eu	4.81-4.82	3.8567	3.8586(6)	7056.80(3)	0.003	0.001	0.749	0.293	4.798	0.093
HD 159376	44850	17 35 15.80	-22 02 37.7	B9 Si	6.46-6.50	9.75	9.738(2)	7134.70(9)	0.020	0.008	0.250	0.300	6.410	0.118
HD 162613	45910	17 53 30.00	-36 30 30.8	A0 Si	7.97-8.01	3.5832	3.5821(3)	7116.75(3)	0.019	0.005	0.046	0.990	7.940	0.042
HD 166053	46770	18 09 36.66	-19 21 27.0	B9 Si	8.32-8.43	3.6043	3.6054(5)	7151.54(3)	0.054	0.005	0.216	0.619	8.288	0.248
HD 166469	46860	18 11 58.16	-28 54 05.5	A0 Si Cr Sr	8.51-8.52	2.8855	2.8890(3)	7121.58(2)	0.006	0.001	0.619	0.805	6.472	0.040
HD 170000	47620	18 20 45.38	+71 20 16.0	A0 Si	4.25-4.27	1.71646	1.71665(9)	7135.57(1)	0.012	0.004	0.132	0.274	-	-
HD 168856	47330	18 22 10.82	-07 29 55.8	B9 Si	7.04-7.07	2.427	2.4277(1)	7060.80(2)	0.013	0.007	0.139	0.024	6.959	0.270
HD 169952	47600	18 25 23.11	+38 26 27.2	B9 Si	7.34-7.37	2.1223	2.12296(8)	7070.69(2)	0.011	0.001	0.183	0.515	7.319	-0.080
HD 171184	47930	18 33 50.81	-14 25 32.9	A0 Si	7.88-7.93	2.70926	2.798(2)	7120.66(2)	0.022	0.009	0.702	0.554	7.825	0.401
HD 172977	48501	18 41 40.21	+34 05 55.5	B9 Si	7.40-7.44	2.2791	2.2799(1)	7067.84(2)	0.017	0.005	0.565	0.814	7.386	-0.189
HD 173650	48660	18 45 35.62	+21 59 05.0	A0 Si Sr Cr	6.49-6.53	9.975	9.976(2)	7058.26(9)	0.020	0.006	0.202	0.628	6.476	0.075
HD 173406	48570	18 45 53.23	-18 21 50.8	B9 Si	7.40-7.45	<b>5.0945</b>	<b>4.5627(4)</b>	7120.59(4)	0.014	0.010	0.200	0.507	7.366	0.197
HD 173657	48690	18 47 37.16	-28 16 47.0	B9 Si Cr	7.39-7.41	1.93789	1.9378(1)	7124.77(1)	0.013	0.003	0.986	0.204	7.367	0.207
HD 174646	48910	18 51 37.93	-01 02 39.9	B9 Si	8.19-8.22	<b>1.1807</b>	<b>6.4193(8)</b>	7124.69(6)	0.012	0.006	0.907	0.942	8.189	0.138
HD 177410	49490	18 58 52.61	+69 31 52.5	B9 Si	6.49-6.52	1.1232524	1.12318(3)	7131.57(1)	0.010	0.008	0.279	0.819	6.458	-0.191
HD 176582	49280	18 59 12.29	+39 13 02.3	B5 He wk.	6.39-6.41	1.58193	1.58221(5)	7057.81(1)	0.010	0.005	0.019	0.264	6.383	-0.232
HD 178591	49677	19 07 19.19	+41 03 14.7	B5 Si	7.10-7.15	4.9396	4.9404(5)	7117.02(4)	0.011	0.022	0.084	0.647	7.114	-0.026
HD 178929	49744	19 11 19.28	-20 20 50.2	B8 Si Sr	7.68-7.75	3.3453	3.3444(2)	7128.75(3)	0.032	0.003	0.241	0.525	7.677	0.010
HD 180029	49955	19 14 45.83	+07 37 12.4	A2 Si	7.71-7.74	3.2858	3.2857(2)	7099.76(3)	0.015	0.004	0.867	0.271	7.946	0.250
HD 184905	51000	19 34 43.92	+43 56 45.1	A0 Si Cr	6.59-6.63	1.84534	1.84548(7)	7068.79(1)	0.017	0.008	0.426	0.095	6.599	-0.020
HD 185183	51130	19 38 56.22	-28 36 25.8	B9 Si	6.70-6.74	1.737	1.73776(6)	7167.58(1)	0.020	0.005	0.270	0.328	6.687	-0.091
HD 187128	51570	19 47 39.75	+15 54 27.6	B9 Si Sr	7.58-7.59	6.1858	6.1880(8)	7085.42(6)	0.005	0.002	0.597	0.899	7.579	0.034
HD 187473	51690	19 51 10.24	-27 28 19.3	B9 Eu Sr Si	7.26-7.36	4.718	4.7184(2)	7176.56(4)	0.040	0.021	0.743	0.844	7.283	-0.035
HD 191287	53290	20 09 41.98	-18 20 48.0	B9 Eu	8.08-8.26	1.62345	1.62342(5)	7137.71(1)	0.087	0.030	0.040	0.327	8.188	0.082
HD 191980	53520	20 12 03.85	+15 21 28.1	B5 He wk.	7.89-7.91	<b>19.5</b>	<b>20.15(1)</b>	7098.5(2)	0.014	0.005	0.616	0.010	7.876	-0.190
HD 192913	53840	20 16 27.20	+27 46 34.0	A0 Si Cr	6.62-6.66	16.846	16.835(5)	7126.6(1)	0.018	0.006	0.403	0.125	6.620	-0.047
HD 193325	53960	20 19 00.95	+20 27 50.9	B9 Si	7.50-7.52	3.1529	3.1520(3)	7129.73(3)	0.010	0.004	0.917	0.695	7.471	-0.183
HD 193722	54060	20 19 56.05	+46 50 14.5	B9 Si	6.45-6.51	<b>1.132854</b>	<b>8.530(1)</b>	7091.65(8)	0.029	0.004	0.390	0.016	6.426	-0.069
HD 196502	54780	20 31 30.42	+74 57 16.6	A2 Sr Cr Eu	5.17-5.19	20.2747	20.31(1)	7160.3(2)	0.003	0.007	0.179	0.699	5.143	0.123
HD 196270	54710	20 35 06.20	+33 33 08.6	B9 Si	8.16-8.21	1.3021519	1.30209(3)	7095.73(1)	0.020	0.009	0.228	0.804	8.188	-0.017
HD 197374	55020	20 41 37.07	+43 50 12.3	B9 Si	8.33-8.36	1.98413	1.98363(8)	7076.81(1)	0.018	0.002	0.152	0.092	8.338	-0.055
HD 197451	55040	20 43 56.96	-05 35 24.8	F1 Sr Eu Cr	7.17-7.20	1.803	1.80268(6)	7139.71(1)	0.012	0.004	0.284	0.313	7.114	0.453
HD 199180	55460	20 55 02.19	+17 15 34.4	A0 Si Cr	7.83-7.85	33.45	33.40(3)	7120.3(3)	0.012	0.003	0.983	0.177	7.822	0.081
HD 199728	55630	20 59 36.14	-19 02 07.0	B9 Si	6.24-6.29	2.2411	2.2400(1)	7194.70(2)	0.018	0.018	0.671	0.090	6.232	-0.121
HD 200177	55750	21 00 06.62	+48 40 46.0	A1 Cr Sr Eu	7.32-7.34	1.47	1.46937(4)	7120.74(1)	0.008	0.002	0.574	0.892	7.317	0.014
HD 200311	55810	21 01 14.32	+43 43 18.5	B9 Si Cr Hg	7.68-7.70	25.96728	26.13(2)	7084.9(2)	0.012	0.002	0.605	0.665	7.658	-0.102
HD 201834	56290	21 10 15.56	+53 33 47.2	B9 Si	5.74-5.75	3.53544	3.5388(5)	7137.45(3)	0.005	0.001	0.849	0.698	5.714	-0.139
HD 203819	56750	21 22 43.03	+54 13 50.4	A0 Cr Si Sr	7.85-7.87	2.58	2.5765(2)	7147.67(2)	0.009	0.005	0.567	0.234	7.846	0.060
HD 205938	57340	21 35 25.92	+68 13 09.3	B9 Si	6.43-6.48	8.34	8.335(1)	7137.54(8)	0.022	0.009	0.353	0.990	6.433	-0.088
HD 206028	57370	21 38 45.78	+24 23 53.5	A0 Si	8.14-8.17	<b>0.785856</b>	<b>3.7092(3)</b>	7139.61(3)	0.015	0.004	0.846	0.421	8.118	-0.103
HD 207188	57640	21 47 36.42	-17 17 41.1	A0 Si	7.63-7.69	2.6733	2.6735(1)	7194.67(2)	0.015	0.016	0.675	0.498	7.649	-0.120
HD 208835	58070	21 57 51.37	+46 51 51.8	B9 Si	7.54-7.56	1.71677	1.71667(9)	7145.71(1)	0.010	0.000	0.215	0.788	7.525	-0.034
HD 210071	58470	22 06 13.56	+56 20 36.3	B9 Si Cr Hg	6.36-6.41	1.43246	1.43264(4)	7147.65(1)	0.015	0.013	0.766	0.387	6.346	-0.105
HD 212939	59060	22 26 55.18	+49 42 43.0	A0 Si	8.14-8.18	2.3934	2.3912(1)	7148.69(2)	0.018	0.001	0.131	0.583	8.149	0.053
HD 213871	59320	22 33 37.58	+46 33 55.0	B9 Si	7.35-7.40	1.9505	1.95070(8)	7183.53(1)	0.023	0.007	0.203	0.702	7.339	0.007
HD 215038	59450	22 39 22.90	+75 39 27.4	B9 Si	8.13-8.18	2.037638	2.03725(8)	7141.71(1)	0.025	0.003	0.228	0.326	8.119	0.002
HD 216533	59810	22 52 41.92	+58 48 23.4	A1 Sr Cr Si	7.86-7.89	17.22	17.256(6)	7150.4(1)	0.013	0.001	0.360	0.158	7.864	0.146
HD 217833	60													

## APPENDIX B: LIGHT CURVES

In this section, the light curves of all objects are presented, folded with the periods listed in Tables [A1](#), [A2](#) and [3](#). Because of the high number of data points, a five-point-binning was applied to the MASCARA data for the construction of the phase plots to increase clarity. The complete light curve figures are available from the authors and in the final publication.

This paper has been typeset from a  $\text{\TeX}/\text{\LaTeX}$  file prepared by the author.

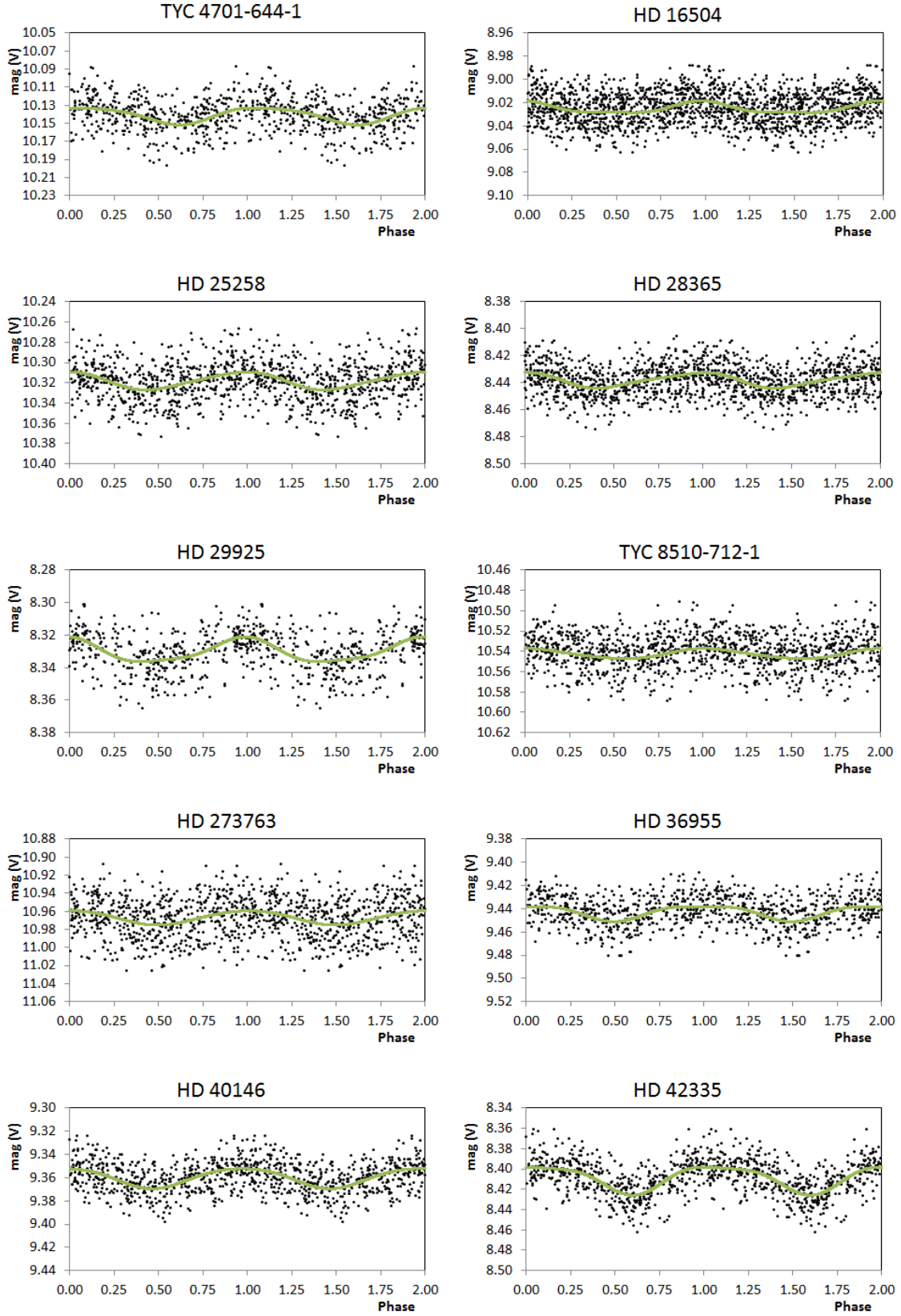


**Figure B1.** Light curves of all stars analyzed with ASAS-3 data, folded with the periods listed in Table A1. The fit curves corresponding to the light curve parameters given in the same table are indicated by the solid lines.